EUROPEAN ORGANIZATION FOR NUCLEAR RESEARCH

CERN-PPE/91-14
24 January 1991

RESULTS FROM LEP AND THE SLC

F. Dydak
CERN, Geneva, Switzerland

Abstract

In this report, the data which became available in the first year of operation of the SLC at SLAC, and, in particular, of LEP at CERN, are reviewed. Most of the quoted results represent the status at the time of the Singapore Conference. However, recent results which have been published until the end of 1990, are incorporated in this report.

Rapporteur's talk given at the
25th International Conference on High Energy Physics

Singapore, 2–8 August 1990

1 Status of LEP and of the SLC

CERN's Large Electron–Positron Collider (LEP) was commissioned in August 1989, and was in operation for three months during the autumn of 1989. In 1990, LEP had already been in operation another four and a half months at the time of the Singapore Conference, with one more month to go until its 1990 shut down. The score of hadronic Z decays recorded on tape is given in Table 1. The

Table 1: Number of hadronic Z decays recorded by the LEP experiments in 1989 and 1990 (in units of 10^3)

	Up to August 1990	Up to the 1990 shut-down
ALEPH	125	185
DELPHI	95	140
L3	90	140
OPAL	120	175

performance of LEP improved steadily with time: the maximum luminosity was $7\times10^{30}\mathrm{cm}^{-2}\mathrm{s}^{-1}$, the typical luminosity during physics data taking was $3\times10^{30}\mathrm{cm}^{-2}\mathrm{s}^{-1}$, to be compared with the design luminosity of $16\times10^{30}\mathrm{cm}^{-2}\mathrm{s}^{-1}$. The combined operation efficiency of LEP and its associated injector complex was 47%, in comparison with a theoretical maximum of 85%. The typical life time of the circulating beams was 20 hours. The integrated LEP luminosity as calculated from the beam currents, as a function of the running time in 1989 and 1990, is shown in Fig. 1. Altogether,

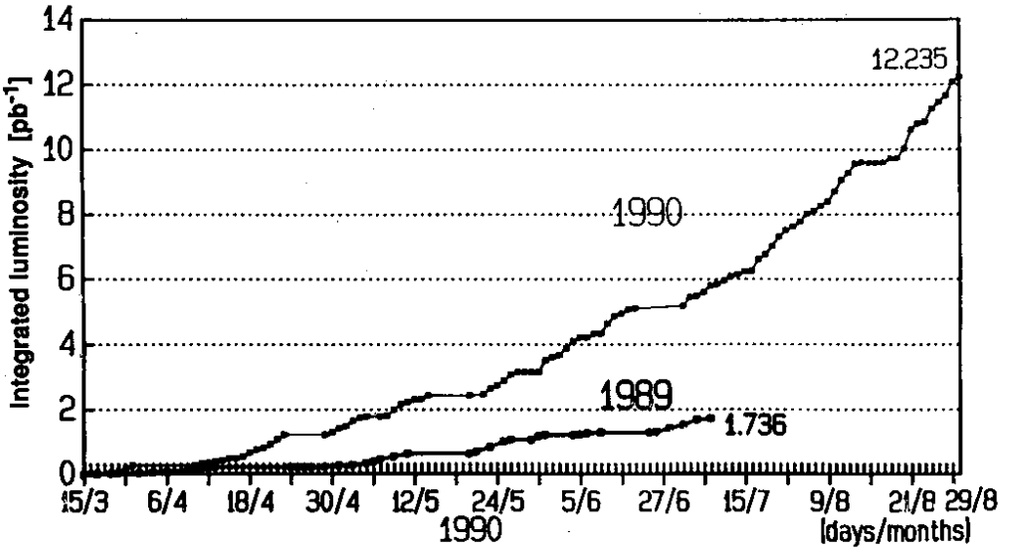

Figure 1: Integrated LEP luminosity as calculated from the beam currents, as a function of the running time in 1989 and 1990

the performance of LEP was satisfactory even though the number of recorded events fell short by a factor of 3 with respect to optimistic hopes. The main reasons for the shortfall were the operation efficiency which was less good than expected, and the beam–beam effect which limited the luminosity already at lower beam currents than anticipated. This latter phenomenon is believed

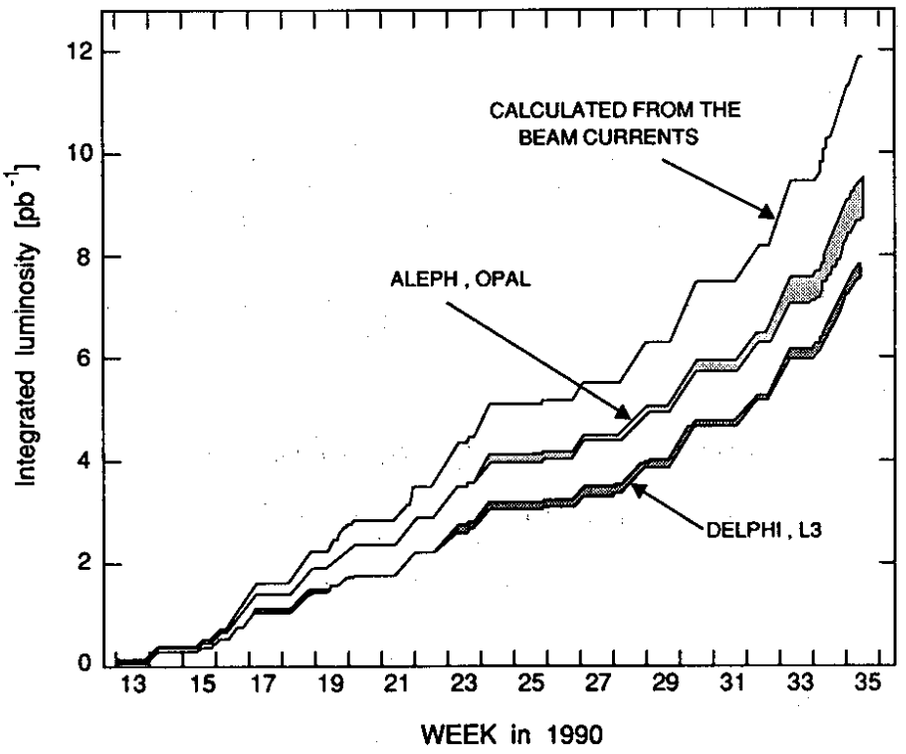

Figure 2: Integrated LEP luminosity in 1990 as a function of the running time, as calculated from the beam currents and as measured by the four LEP experiments

to be caused by bad luck in the choice of the machine tune. Hence the search for a better machine tune constitutes the top priority in the 1991 machine development programme.

The loss in luminosity due to the beam–beam effect was about 20% during the 1990 run, as can be seen from the difference of the luminosity calculated from the beam currents, and the one measured by ALEPH and OPAL (see Fig. 2). The different numbers of events recorded by the four LEP experiments are mainly due to an asymmetry in the machine luminosity, which favoured ALEPH and OPAL by 20% with respect to DELPHI and L3 (see Fig. 2). Shortly before the 1990 shut down, the origin of this asymmetry was recognized, and equal luminosities for the four experiments were achieved. The results from LEP which have been published so far, and which have been presented at the Singapore Conference, did not necessarily make use of the total statistics which are given in Table 1. Differences in the experimental errors quoted by the four LEP experiments, and differences in the mass limits on new particles, are normally due to data samples of different size.

As for 1991, the combination of a longer running time ($\times$ 1.5), higher beam currents ($\times$ 1.5), and higher operation efficiency ($\times$ 1.4), should yield an overall improvement by a factor of 3 with respect to the 1990 score of events, that is some 500×10^3 hadronic Z decays per experiment.

SLAC's Linear Collider, the SLC, had its first physics run before LEP, in the spring of 1989. First results were presented at the 1989 Lepton–Photon Conference [1]. Then the accelerator was badly struck by the earthquake which took place in California on 17 October, 1989. The accelerator again came into operation in July 1990, with the MARK II detector taking data. The total score of hadronic Z decays was 450 in 1989, and 250 more from the 1990 running. By the end of 1990, MARK II was replaced by a newly built detector, the SLD. From 1991 onwards, operation with longitudinally polarized electron beams will be a focal point of interest.

2 Electroweak physics

2.1 Introduction

The precise measurement of the Z line shape and the Z decay characteristics has attracted a lot of attention. We recall here the basic formulae, with a view to introducing our nomenclature. In Born approximation, the $e^+e^- \to f\bar{f}$ matrix element reads as follows:

$$\mathcal{M} = Q_e Q_f \frac{4\pi\alpha}{s} J_e^{\rm em} J_f^{\rm em} + \sqrt{2}\rho G_{\rm F} m_Z^2 \frac{1}{s - m_Z^2 + i m_Z \Gamma_Z} (J_e^3 - 2\sin^2\theta_{\rm w} J_e^{\rm em})(J_f^3 - 2\sin^2\theta_{\rm w} J_f^{\rm em}) ,$$

with the fermion current

$$J_f^3 - 2\sin^2\theta_{\rm w} J_f^{em} = \bar{u}_f[\gamma_\mu(I_f^3 - 2Q_f \sin^2\theta_{\rm w}) + \gamma_\mu\gamma_5 I_f^3]v_f ,$$

and the vector and axial-vector coupling constants, defined as

$$g_{{\rm V}f} = I_f^3 - 2Q_f \sin^2\theta_{\rm w}$$

$$g_{{\rm A}f} = I_f^3 .$$

The Veltman parameter

$$\rho = \frac{G_{\rm F}^{\rm NC}}{G_{\rm F}^{\rm CC}} = \frac{m_W^2}{m_Z^2 \cos^2\theta_{\rm w}}$$

is equal to unity in the Minimal Standard Model (MSM), and the definitions of the electroweak mixing parameter via the W and Z masses, and via the electromagnetic and weak coupling constants, coincide in Born approximation:

$$\sin^2\theta_{\rm w} = 1 - \frac{m_W^2}{m_Z^2} = \frac{e^2}{g^2} .$$

As is well known, electroweak radiative corrections are large compared with the experimental errors. We are very fortunate that a tremendous amount of theoretical work has been done in preparation for Z physics, a work without which the many high-precision results from LEP would have been impossible. Notice that since 1973 some 1500 papers on the subject have been published, by some 100 authors!

Electroweak radiative corrections are customarily divided into two categories:

- *Photonic corrections*

  They involve in first order an extra photon which is added to the Born diagrams, either in the form of a real bremsstrahlung photon, or as a virtual photon loop. The corrections are very large, of the order of 100%, and depend on the experimental cuts. The dominant contribution is due to initial-state bremsstrahlung, and is customarily represented by a radiator fuction $\mathcal{H}(z,s)$ which is folded with the Born cross-section. For example, the Z line shape then takes the form

  $$\sigma^f(s) = \int_0^1 \sigma_f^0(zs)\mathcal{H}(z,s)dz .$$

  Figure 3 shows a sample of diagrams of photonic corrections.

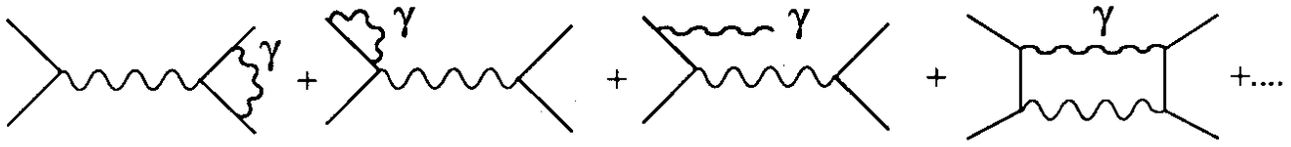

Figure 3: Diagrams of photonic corrections

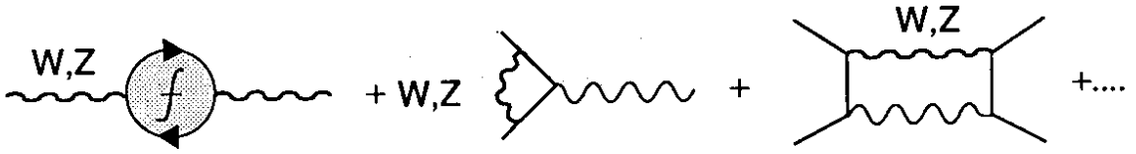

Figure 4: Diagrams of non-photonic corrections

- *Non-photonic corrections*

  They involve all other corrections, notably the self-energy corrections of the vector bosons, and virtual W and Z loops (see Fig. 4). These corrections are still large – of the order of 10% – but independent of experimental cuts. The bulk of these non-photonic corrections can be absorbed into 'running' (i.e. Q^2-dependent) coupling constants, while preserving the Born approximation formulae. This concept, which has been pioneered by Kennedy and Lynn [2], has become known as the 'improved Born approximation' [3].

Throughout this report, the improved Born approximation and the notion of running coupling constants are utilized for presenting and interpreting the data. All formulae given below are understood to be valid only in the improved Born approximation: in each case a small correction is being ignored. The present level of the experimental accuracy still permits this approach; however in the future a more rigorous treatment will be needed when it comes to analysing many millions of Z decays.

The Z line shape for the final-state fermion f reads as follows:

$$\sigma_f(s) = \frac{s}{(s-m_Z^2)^2 + \frac{s^2\Gamma_Z^2}{m_Z^2}} \left(\frac{12\pi}{m_Z^2}\Gamma_e\Gamma_f + I_f N_c \frac{s-m_Z^2}{s} \right) + \frac{4\pi}{3} N_c Q_f^2 \frac{\bar{\alpha}^2}{s} ,$$

where I_f denotes the Z–γ interference term, and $\bar{\alpha}$ the fine structure constant at $Q^2 = m_Z^2$. The Z mass and widths are understood as the physical line shape parameters. The decay width for the fermion f is

$$\Gamma_f = \frac{G_F m_Z^3}{6\sqrt{2}\pi} (\bar{g}_{Vf}^2 + \bar{g}_{Af}^2) , \tag{1}$$

with

$$\bar{g}_{Vf} = \sqrt{\bar{\rho}} (I_f^3 - 2Q_f \sin^2 \bar{\theta}_w)$$

and

$$\bar{g}_{Af} = \sqrt{\bar{\rho}} I_f^3 ,$$

where the Fermi constant G_F, unlike other coupling constants, is not running but used with its numerical value $G_F = 1.16637 \times 10^{-5}$ GeV^{-2}.

The forward-backward asymmetry for the fermion f is given by

$$\mathcal{A}_f^{\mathrm{FB}} = \frac{3}{4}\mathcal{A}_e\mathcal{A}_f\,,$$

with

$$\mathcal{A}_e = 2\frac{\bar{g}_{\mathrm{V}e}\bar{g}_{\mathrm{A}e}}{\bar{g}_{\mathrm{V}e}^2 + \bar{g}_{\mathrm{A}e}^2}$$

and

$$\mathcal{A}_f = 2\frac{\bar{g}_{\mathrm{V}f}\bar{g}_{\mathrm{A}f}}{\bar{g}_{\mathrm{V}f}^2 + \bar{g}_{\mathrm{A}f}^2}\,.$$

The W and Z masses are, in terms of running coupling constants, given by

$$m_W^2 = \frac{\pi\bar{\alpha}}{\sqrt{2}G_{\mathrm{F}}\sin^2\bar{\theta}_{\mathrm{w}}}$$

and

$$m_Z^2 = \frac{\pi\bar{\alpha}}{\sqrt{2}\bar{\rho}G_{\mathrm{F}}\sin^2\bar{\theta}_{\mathrm{w}}\cos^2\bar{\theta}_{\mathrm{w}}}\,.$$

The running electroweak mixing parameter, $\sin^2\bar{\theta}_{\mathrm{w}}$, is related to the W and Z masses by

$$\sin^2\bar{\theta}_{\mathrm{w}} = \frac{\bar{e}^2}{\bar{g}^2} = 1 - \frac{m_W^2}{\bar{\rho}m_Z^2}\,.$$

Other definitions of the running weak mixing parameter found in the literature, such as $\sin^2\theta_{\bar{M}S}$, $\sin^2\theta_{\mathrm{w}}(m_Z^2)$, and $\sin^2\theta_w^\star$, are, apart from very small corrections, equivalent. The running Veltman parameter is given by

$$\bar{\rho} = 1 + \Delta\bar{\rho} = 1 + \frac{3\sqrt{2}}{16\pi^2}G_{\mathrm{F}}m_t^2\,,$$

exhibiting a quadratic dependence on the mass of the t quark which permits conclusions on the range of allowed values of m_t.

It is perhaps useful to recall here the (equivalent) definition of m_W in another renormalization scheme which has been widely used in the past, in particular in the analysis of $p\bar{p}$ data:

$$m_W^2 = \frac{\pi\alpha}{\sqrt{2}G_{\mathrm{F}}\sin^2\theta_{\mathrm{w}}(1-\Delta r)}\,,$$

where the coupling constants are not running with Q^2, and the electroweak mixing parameter is given by

$$\sin^2\theta_{\mathrm{w}} = 1 - \frac{m_W^2}{m_Z^2}\,,$$

and all radiative corrections are concentrated in the term

$$\Delta r = \Delta\alpha - \frac{\cos^2\theta_{\mathrm{w}}}{\sin^2\theta_{\mathrm{w}}}\Delta\rho\,,$$

where $\Delta\alpha = \bar{\alpha} - \alpha$.

The procedure which is applied in the data analysis is depicted in Fig. 5. The raw data are corrected for the limited apparatus acceptance and resolution, and other mundane effects such as dead electronic channels. The result are 'perfect' data which can then be confronted with theoretical expectations. The latter start from Born cross-sections, and are modified by applying

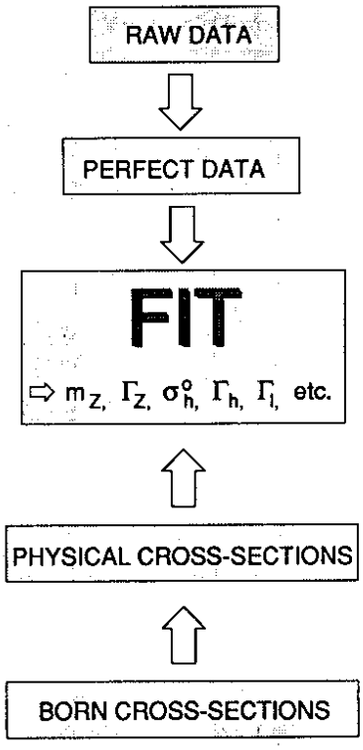

Figure 5: Procedure of the data analysis

photonic and non-photonic radiative corrections leading to physical cross-sections which an ideal apparatus would measure.

A fit of the perfect data to the theoretically expected physical cross-sections leads to the best values of free input parameters such as m_Z, Γ_Z, $\sigma^0_h, \Gamma_h, \Gamma_e, \Gamma_\mu, \Gamma_\tau$, and $\Gamma_{\rm inv}$. The point is that up to this stage the only assumption is a Breit–Wigner form of the Z line shape and the validity of QED for the calculation of the radiator function. Thus, apart from numerically unimportant contributions from the Z–γ interference, and from non-photonic radiative corrections, the procedure leads to determinations of the parameters of the Z line shape which are independent of the MSM.

In the subsequent sections, the results on the Z line shape parameters are presented as determined by the four LEP Collaborations. The errors quoted for the individual experiments are obtained after unfolding all systematic errors that we consider common to all four experiments, and then adding quadratically the remaining, experiment-specific, systematic and statistical errors. This allows a judgement of the compatibility of the results. After averaging, we add our own estimate of the common systematic error, thus obtaining the overall experimental result, which can then be compared with the expectation from the MSM. The latter is calculated by using the program GAMMAZ [4], for the central values $m_Z = 91.18$ GeV, $m_t = 150$ GeV, $m_H = 200$ GeV, and $\alpha_s = 0.115$. The error given for the MSM prediction is obtained by adding quadratically the deviations arising from variations in the range $91.15 \leq m_Z \leq 91.21$ GeV, $80 \leq m_t \leq 250$ GeV, $40 \leq m_H \leq 1000$ GeV, and $0.10 \leq \alpha_s \leq 0.13$.

2.2 Z mass

In the fit of the Z line shape, the Z mass is numerically stable, virtually unaffected by other fit parameters. The statistical precision is dominated by the abundant hadronic decays. Figure 6 shows the Z mass measurements performed by the LEP experiments, from a scan across the resonance at the energies 91.2 ± 0.5, $\pm$ 1, $\pm$ 2, and $\pm$ 3 GeV. The total error is completely dominated by the

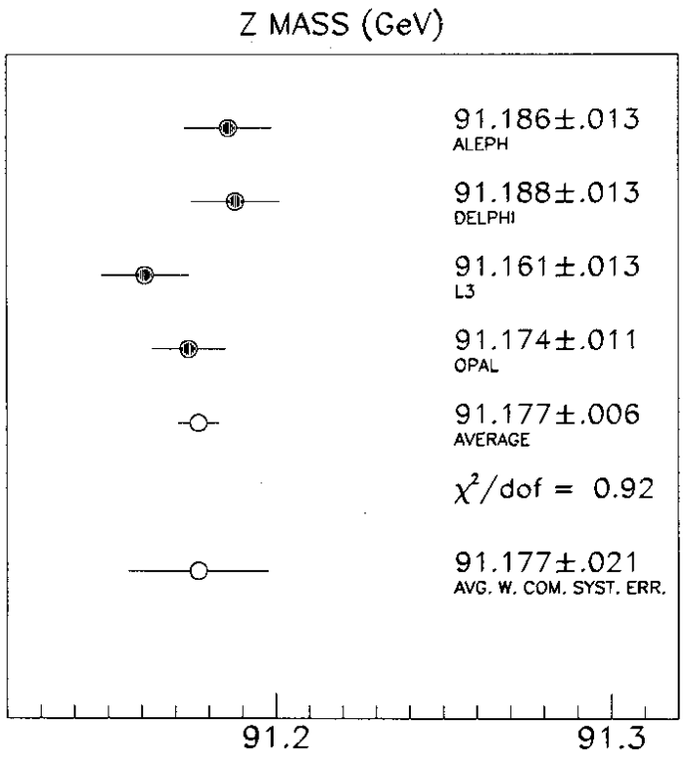

Figure 6: Measurements of the Z mass

uncertainty of the absolute energy calibration of LEP.

The absolute energy scale is based on a measurement of the velocities of positrons and protons circulating with the same momentum of 20 GeV in the machine, resulting in a calibration of the magnetic field at 20 GeV. This calibration is scaled up to 45 GeV with the help of flux-loop measurements. A careful assessment of the measurement errors resulted in an estimate of the absolute scale error at the Z pole of 2.4×10^{-4}, i.e. 22 MeV [5]. This figure suggests, however, a greater precision than warranted: as the dominant contribution to the scale error arises from the distortion of the magnetic field by a few μm thick Ni layer in the beam pipe, the effective thickness of which is not well known, we prefer to quote a round number of 20 MeV as the best guess, available at the moment, for the uncertainty of the machine's centre-of-mass energy at the Z pole.

It is expected that a significant increase in precision of the beam energy will occur during 1991, when the frequency of the electron-spin precession will be measured. The ultimate error of the Z mass is then expected to shrink to about 5 MeV.

The measurements of the Z mass shown in Fig. 6 are in good agreement. The average is 91.177 $\pm$ 0.021 GeV.

2.3 Total width and hadronic peak cross-section

A common fit to the Z line shape as measured with $Z \to q\bar{q}, e^+e^-, \mu^+\mu^-$, and $\tau^+\tau^-$ events permits the simultaneous determination of six resonance parameters which can, for example, be chosen as $m_Z, \Gamma_Z, \sigma_h^0, \Gamma_e/\Gamma_h, \Gamma_\mu/\Gamma_h$, and Γ_τ/Γ_h, a set of reasonably uncorrelated parameters.

As for the total width Γ_Z, the measurements are in good agreement (see Fig. 7). The common systematic error is estimated at $\pm$5 MeV, mostly due to point-to-point errors in the LEP energy settings (recent progress in the understanding of radiative corrections [6] eliminated them as another source of common systematic uncertainty). As can be seen from Fig. 7, the common systematic

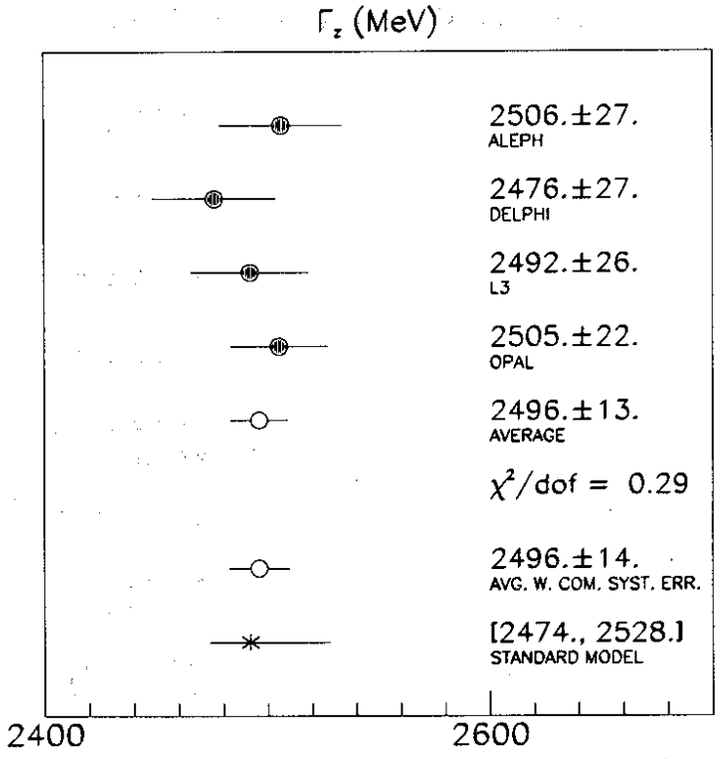

Figure 7: Measurements of the total Z width

error is much smaller than the experimental error, so there is quite some room for improvement in the measurement of Γ_Z. The current average, $\Gamma_Z = 2496 \pm 14$ MeV, is in good agreement with the MSM prediction. The ultimate precision on Γ_Z will be about 5 MeV.

The hadronic peak cross-section (in Born approximation, before radiative corrections),

$$\sigma_h^0 = \frac{12\pi}{m_Z^2}\frac{\Gamma_e\Gamma_h}{\Gamma_Z^2}, \tag{2}$$

is statistically well determined but suffers from a $\pm 1\%$ (± 0.4 nb) error arising from theoretical uncertainties in the Bhabha cross-section, which is utilized to determine the luminosity from the observed $e^+e^- \to e^+e^-$ events at small polar angles. The measurements of σ_h^0 are shown in Fig. 8. They are well compatible, and the average is in good agreement with the MSM prediction.

2.4 Hadronic and leptonic widths

The hadronic widths resulting from common fits to hadronic and leptonic Z decays are displayed in Fig. 9. A common systematic error of $\pm 0.5\%$ (± 9 MeV) due to the theoretical uncertainty of the Bhabha cross-section has been assumed. The measurements are in good agreement, as they are with the MSM prediction. There is room for improvement with further running. The ultimate error on Γ_h will be about 8 MeV.

The measurements of the electronic Z widths are displayed in Fig. 10. As Bhabha scattering proceeds both through s- and t-channel diagrams, an additional, even dominant, systematic uncertainty arises from the theoretical uncertainty of the t-channel subtraction, which is estimated to be $\pm 1\%$ (± 0.8 MeV) of the electronic width. The measurements are in good agreement, and are quite consistent with the MSM prediction. The common systematic error dominates the total error, calling for a better understanding of the Bhabha cross-section, in particular of the t-channel contribution, to make further running more useful.

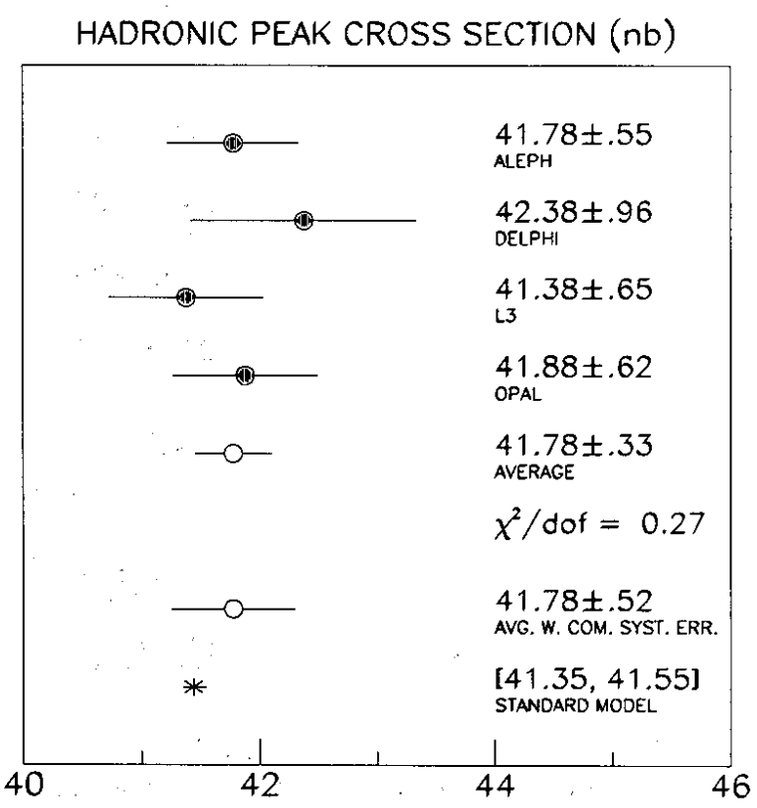

Figure 8: Measurements of the hadronic peak cross-section of the Z

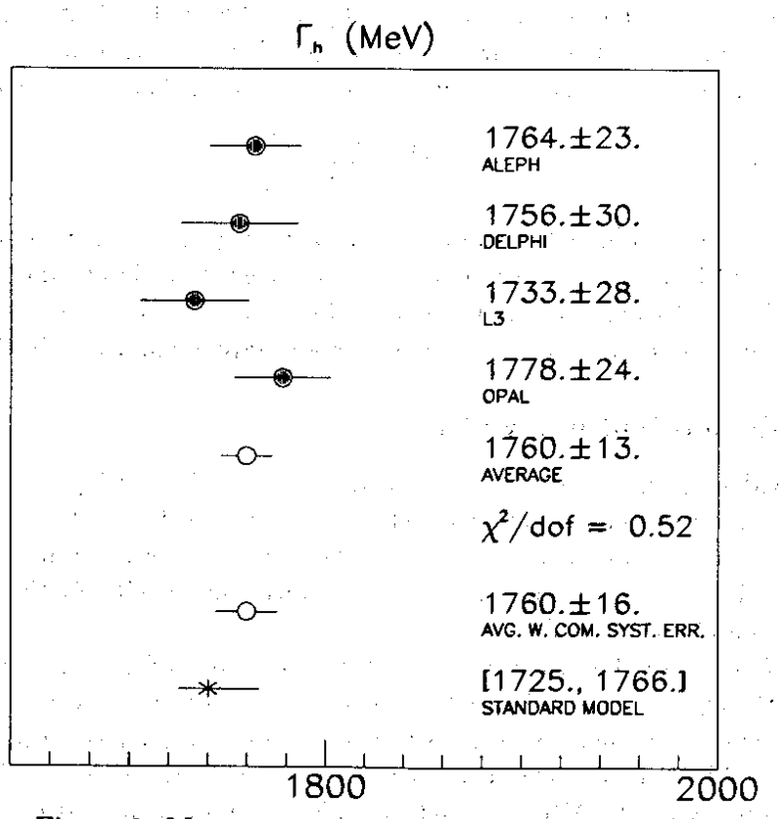

Figure 9: Measurements of the hadronic Z width

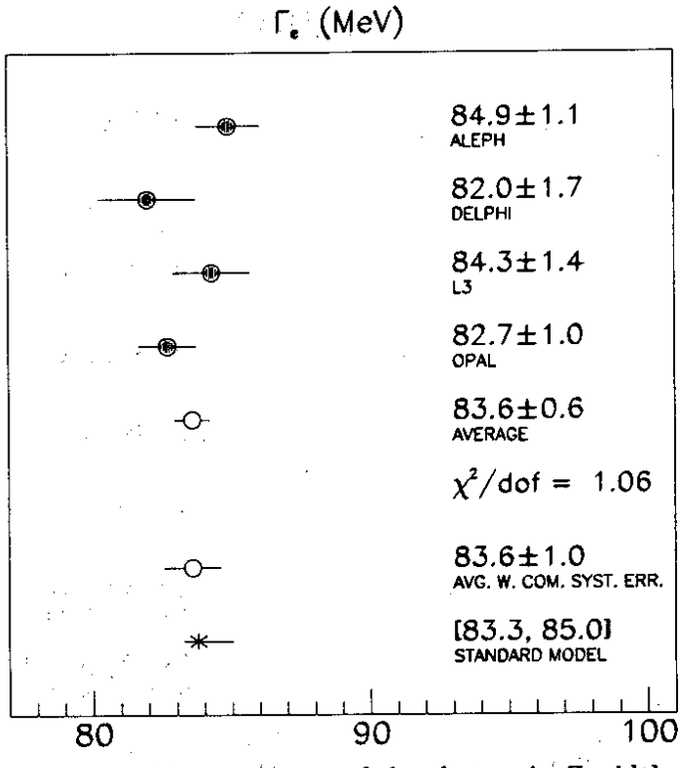

Figure 10: Measurements of the electronic Z width

Figure 11 shows the measurements of the muonic Z width. The common systematic error is smaller than for Γ_e, i.e. ±0.5% (±0.4 MeV), arising from the uncertainty of the Bhabha cross-section. The common systematic error is small compared with the overall error, so that quite some improvement is possible by further running. The measurements are in good agreement as they are with the MSM prediction.

Figure 12 shows the measurements of the tauonic Z width. The common systematic error is the same as for Γ_μ, i.e. ±0.5% (±0.4 MeV) from the uncertainty of the Bhabha cross-section. This error is small compared with the experimental error, and leaves much room for improvement. The measurements are in good agreement as they are with the MSM prediction.

Finally, Fig. 13 displays the measurements of the leptonic width, assuming e-μ-τ universality. The common systematic error is estimated at ±0.6% (±5 MeV) owing to the uncertainty of the Bhabha cross-section and to the t-channel subtraction in large-angle Bhabha scattering. Again, the measurements agree well with each other, and with the MSM prediction. A significant improvement of the measurement requires a better theoretical understanding of Bhabha scattering. The ultimate error on Γ_l will be about 0.3 MeV.

The Z partial widths exhibit a significant dependence on m_t through non-photonic radiative corrections: varying m_t from 60 to 220 GeV increases the partial widths by about 1.5%. As this m_t dependence tends to cancel in ratios of partial widths, quantities such as σ_h^0 (Eq. 2) or $R_{hl} = \Gamma_h/\Gamma_l$ provide a particularly stable testing ground of the MSM. Figure 14 shows the experimental results for R_{hl}. The common systematic uncertainty is estimated to be ±0.3% of R_{hl}, owing to the uncertainty of the t-channel subtraction, which is small compared with the overall experimental error. There is good agreement with the MSM prediction. It will be most interesting to see whether this agreement persists when the error is reduced by further data taking.

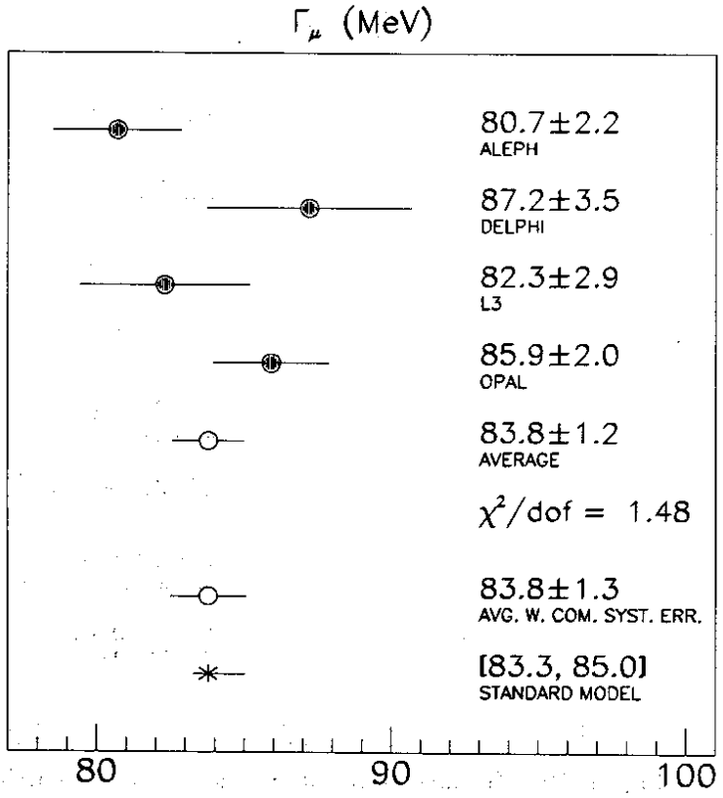

Figure 11: Measurements of the muonic Z width

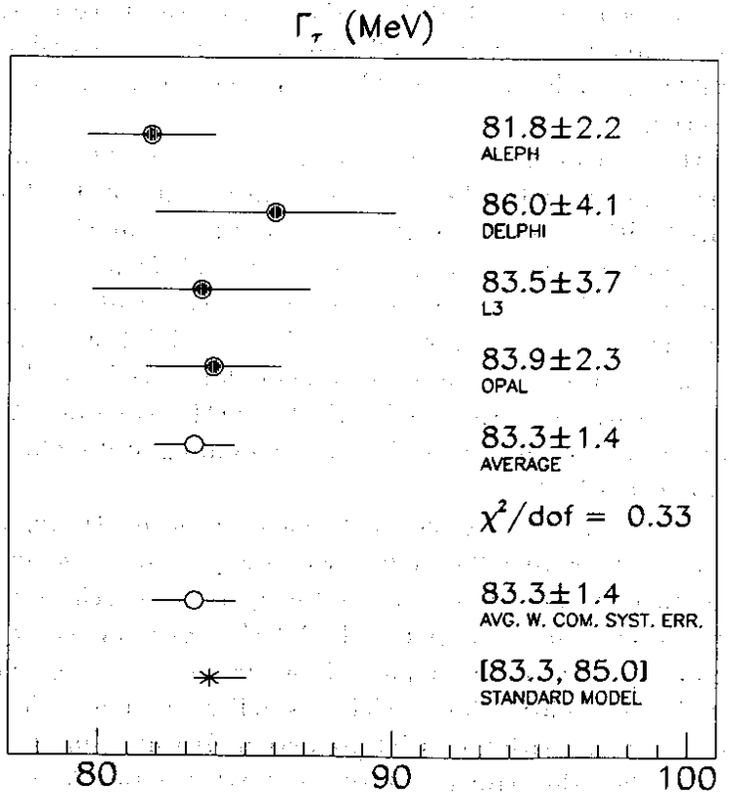

Figure 12: Measurements of the tauonic Z width

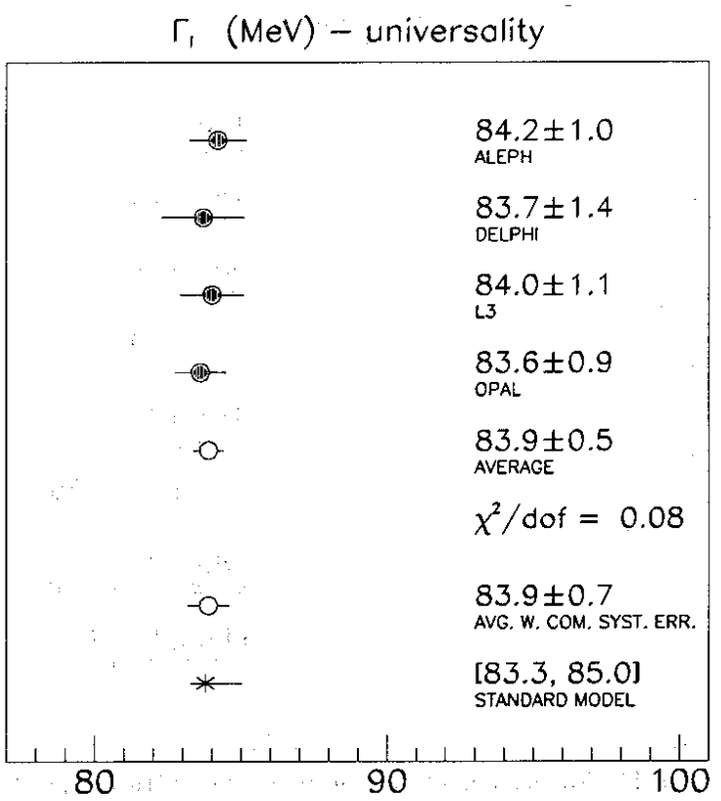

Figure 13: Measurements of the leptonic Z width

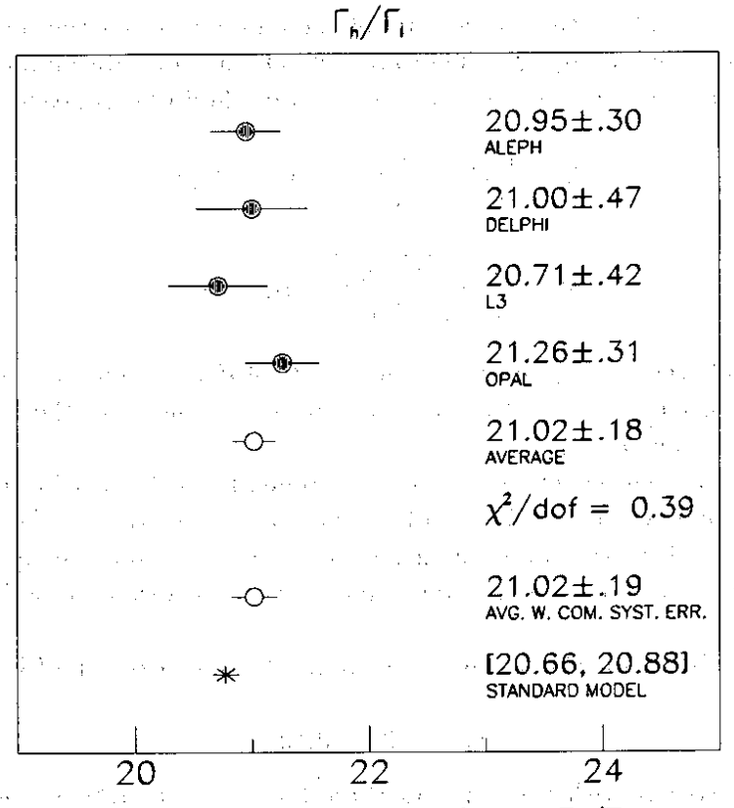

Figure 14: Measurements of $R_{hl} = \Gamma_h/\Gamma_l$

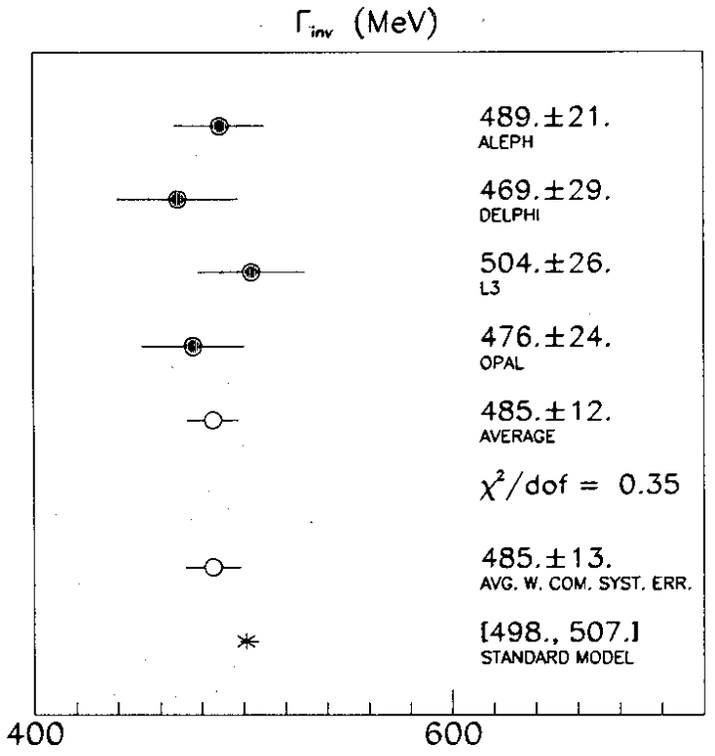

Figure 15: Measurements of the invisible width of the Z

2.5 Invisible width and the number of neutrino families

As is well known, the Z total width is a measure of the number of neutrino families, N_ν, provided the neutrino mass is well below $m_Z/2$. There are several ways of determining N_ν. As statistical precision is no longer the main concern, we choose here a method that is nearly model independent. From

$$N_\nu = \frac{\Gamma_{\rm inv}}{\Gamma_\nu} = \frac{1}{\Gamma_\nu}(\Gamma_Z - \Gamma_h - 3\Gamma_l)\,,$$

we obtain

$$N_\nu = \frac{\Gamma_l}{\Gamma_\nu}\left(\sqrt{\frac{12\pi R_{hl}}{\sigma_h^0 m_Z^2}} - R_{hl} - 3\right). \qquad (3)$$

We utilize in this formula the average of the measurements of R_{hl}, σ_h^0, and m_Z. The only information from the MSM that is needed is the ratio – not the absolute values – of the leptonic and neutrino widths, which is independent of m_t.

Figure 15 shows the measurements of $\Gamma_{\rm inv}$ as determined from the relation $\Gamma_{\rm inv} = \Gamma_Z - \Gamma_h - 3\Gamma_l$, taking properly into account the correlation of the measurement errors. The common systematic error is estimated at ±5 MeV, stemming mainly from the point-to-point errors in the LEP energy settings. The measurements are in good agreement with each other, as well as with the MSM prediction.

Utilizing Eq. 3 we obtain for the number of neutrino families from the LEP measurements the average

$$N_\nu = 2.90 \pm 0.10\,.$$

This value is quite consistent with the belief in three families of quarks and leptons with next to mass-less neutrinos, but has also given rise to speculations as to the existence of right-handed neutrinos [7]. As the common systematic error in $\Gamma_{\rm inv}$ is small compared with the overall experimental

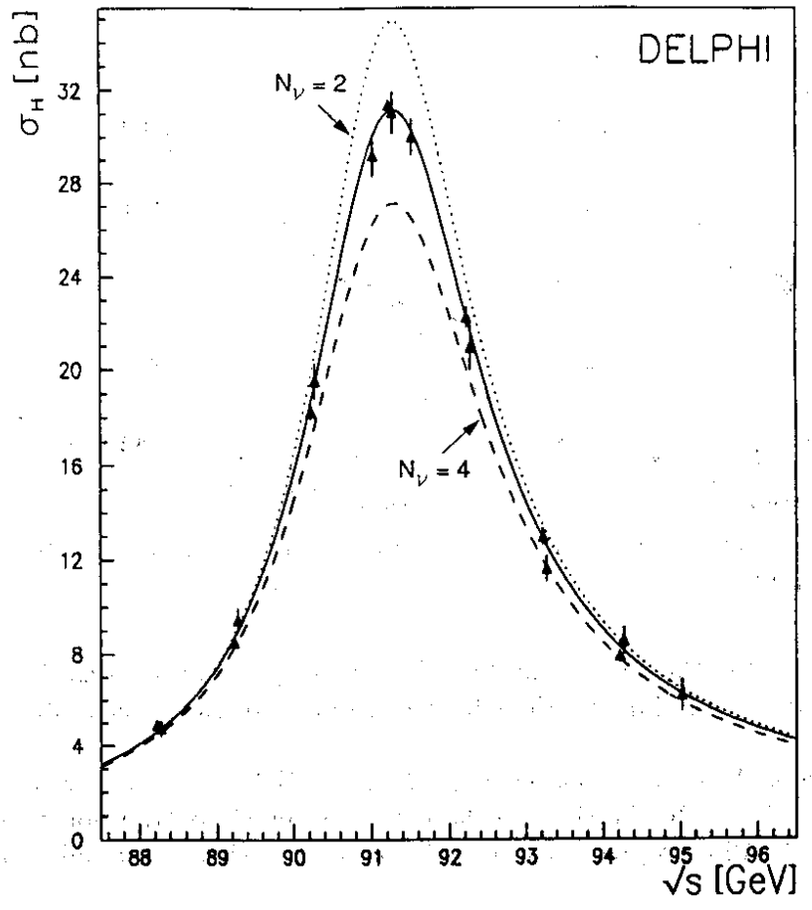

Figure 16: Measurement of the Z line shape, and comparison with the MSM expectation for N_ν = 2, 3, and 4 (DELPHI)

error, a significant improvement of N_ν is expected from further running. Ultimately, the number of neutrino families will be measured to ± 0.03 ($\pm 1\%$).

Figure 16 shows the most prominent achievement in the first year of data taking at LEP: the precise mapping of the Z line shape as measured with hadronic events. The data are quite consistent with $N_\nu = 3$, whereas $N_\nu = 2$ and $N_\nu = 4$ are clearly ruled out. The data shown in Fig. 16 are from the DELPHI experiment. The analogous data from the ALEPH, L3, and OPAL experiments look of course equally convincing.

2.6 Forward–backward asymmetry of leptons

With the exception of L3, who studied electrons and muons only, the LEP experiments presented results on the forward–backward asymmetry of electrons, muons, and taus, for all energies which have been employed during the scan of the Z resonance.

On the peak, the leptonic forward–backward asymmetry is given in the improved Born approximation by

$$A_l^{\mathrm{FB}} = \frac{3}{4}\mathcal{A}_e\mathcal{A}_l\,,$$

with

$$\mathcal{A}_l = 2\frac{\bar{g}_{\mathrm{V}l}\bar{g}_{\mathrm{A}l}}{\bar{g}_{\mathrm{V}l}^2 + \bar{g}_{\mathrm{A}l}^2}\,.$$

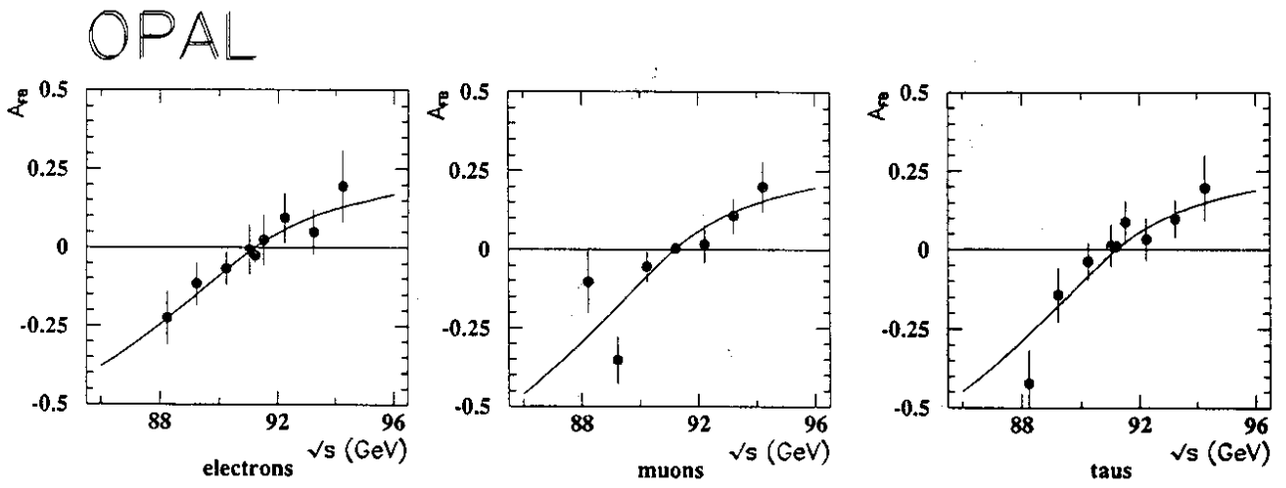

Figure 17: Forward–backward asymmetry of electrons, muons, and taus as a function of the centre-of-mass energy (OPAL)

From the measurement of the forward–backward asymmetry of leptons, together with the measurement of the leptonic width (Eq. 1), the effective leptonic coupling constants $\bar{g}_{Vl}$ and $\bar{g}_{Al}$ can be determined.

As an example of the data presented, Fig. 17 shows A_l^{FB} separately for electrons, muons, and taus as a function of $\sqrt{s}$. In the electron data, the t-channel contribution to Bhabha scattering has been subtracted. All data presented are well compatible with lepton universality, and with the MSM prediction.

2.7 Forward-backward asymmetry of b quarks.

ALEPH and L3 measured the forward–backward asymmetry of b quarks through their semileptonic decays into both electrons and muons, whereas OPAL confined themselves to muons only.

The forward–backward asymmetry of the $Z \rightarrow b\bar{b}$ decay is given by

$$A_b^{FB} = \frac{3}{4}\mathcal{A}_e\mathcal{A}_b \,,$$

with

$$\mathcal{A}_b = 2\frac{\bar{g}_{Vb}\bar{g}_{Ab}}{\bar{g}_{Vb}^2 + \bar{g}_{Ab}^2} \,.$$

Owing to $b\bar{b}$ mixing, the observed forward–backward asymmetry is smaller than the true asymmetry:

$$A_b^{FB} = \frac{A^{obs}}{1-2\chi} \,,$$

where χ denotes the probability of a b quark turning into a $\bar{b}$ quark, over the entire decay time. The isolation of $b\bar{b}$ events is performed by selecting leptons with high momentum and high p_T with respect to the nearest hadronic jet. The efficiency of this selection can be judged from Fig. 18, which shows the p_T spectrum of electron candidates, together with the Monte Carlo expectations from various sources (L3 data). The sample of events with, say, $p_T > 2$ GeV, has a small background only.

Figure 19 shows, as an example, the ALEPH data on the polar angle distribution of $b\bar{b}$ events.

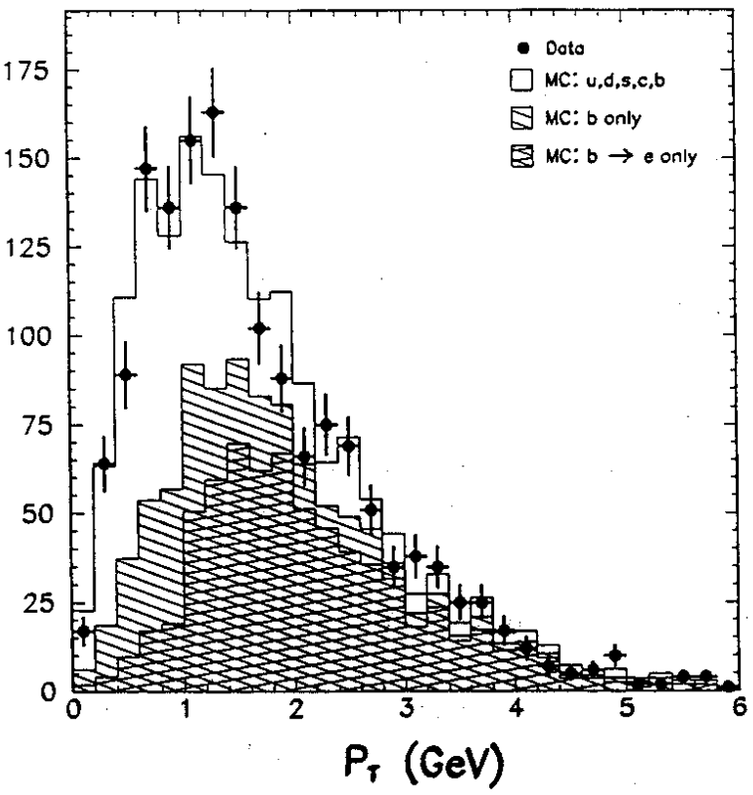

Figure 18: p_T distribution of electron candidates in Z hadronic events (L3)

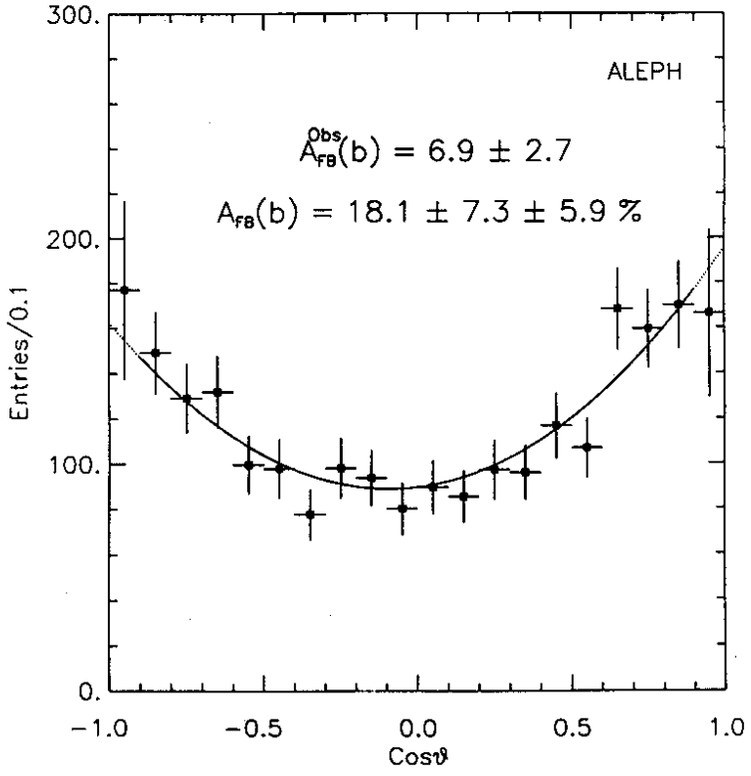

Figure 19: Polar-angle distribution of $b\bar{b}$ events (ALEPH)

Table 2: Measurements of $A_b^{\rm FB}$, corrected for $b\bar{b}$ mixing (the OPAL measurement has been corrected by the author, using $\chi = 0.13 \pm 0.04$)

	$A_b^{\rm FB}$
ALEPH (e, μ) [8]	0.181 ± 0.094
L3 (e, μ) [9]	$0.130^{+0.044}_{-0.042}$
OPAL (μ only) [10]	0.03 ± 0.12
MSM prediction ($m_t = 100$ GeV)	0.103

Table 2 lists the measurements of $A_b^{\rm FB}$, together with the MSM prediction. Further data taking is expected to lead to significant improvements in the precision of $A_b^{\rm FB}$, which is of quite some interest as $A_b^{\rm FB}$ is a sensitive measure of $\sin^2\bar{\theta}_{\rm w}$ (for example, the ALEPH result $A_b^{\rm FB} = 0.181 \pm 0.094$ corresponds to $\sin^2\bar{\theta}_{\rm w} = 0.218 \pm 0.017$).

2.8 Charge asymmetry of hadronic jets

ALEPH have measured the charge asymmetry of hadronic jets, summed over all five quark flavours. For each quark flavour f, let $\vec{n}_T$ be the unit vector in the jet's thrust direction; weighting the charge Q_i of the i-th track with the longitudinal momentum component along the thrust direction, we obtain the weighted jet charge for the quark flavour f,

$$Q_f = \frac{\sum_i Q_i |\vec{p}_i \vec{n}_T|^\kappa}{\sum_i |\vec{p}_i \vec{n}_T|^\kappa} ,$$

where the exponent κ has an empirically determined optimum value close to unity. We define the charge asymmetry for the quark flavour f,

$$A_f^Q = Q_f \frac{\sigma_f^F - \sigma_f^B}{\sigma_f^F + \sigma_f^B} = Q_f A_f^{\rm FB} ,$$

and the charge asymmetry for all quark flavours,

$$A_h^Q = \sum_f Q_f A_f^{\rm FB} \frac{\Gamma_f}{\Gamma_h} .$$

In terms of the relevant effective coupling constants, we obtain

$$A_h^Q \simeq const \frac{\bar{g}_{{\rm V}e}}{\bar{g}_{{\rm A}e}} \sum_f Q_f \bar{g}_{{\rm V}f} \bar{g}_{{\rm A}f} .$$

Taking the jet charge Q_f from a Monte Carlo simulation of quark jets with flavour f, and the effective coupling constants $\bar{g}_{{\rm V}f}$ and $\bar{g}_{{\rm A}f}$ from neutrino–nucleon scattering experiments (employing universality of quark families), the charge asymmetry A_h^Q determines the ratio $\bar{g}_{{\rm V}e}/\bar{g}_{{\rm A}e}$, including the relative sign of the leptonic vector and axial-vector coupling constants.

ALEPH measured [11]

$$A_h^Q = -0.0107 \pm 0.0023 ,$$

resulting in

$$\frac{\bar{g}_{{\rm V}e}}{\bar{g}_{{\rm A}e}} = 0.090 \pm 0.031 .$$

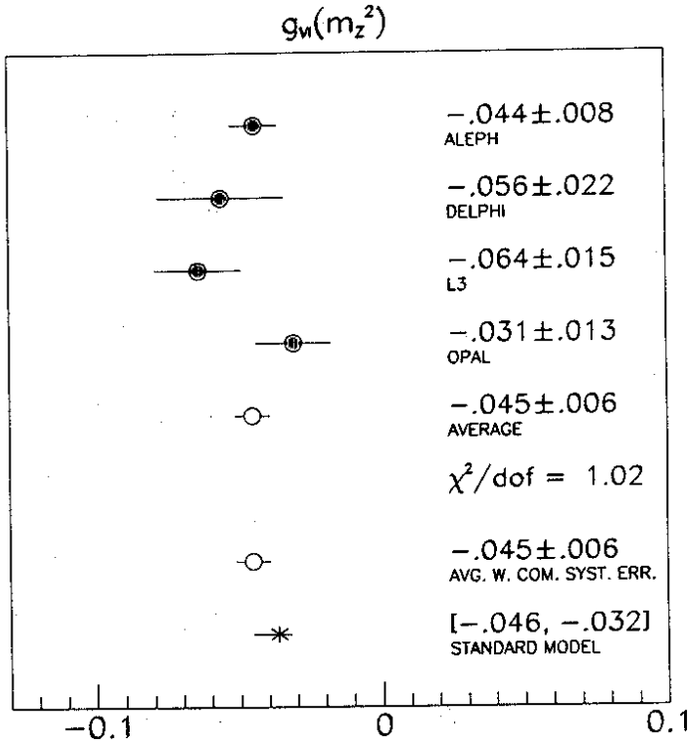

Figure 20: The leptonic vector coupling constant

2.9 τ polarization.

ALEPH measured the τ polarization in $e^+e^- \to \tau^+\tau^-$ events, by analysing the momentum spectrum in $\tau \to \pi\nu_\tau, \mu\bar{\nu}_\mu\nu_\tau$, and $A_1\nu_\tau$ decays. The result for the τ polarization is [12]

$$\mathcal{P}_\tau = 2\frac{\bar{g}_{V\tau}\bar{g}_{A\tau}}{\bar{g}_{V\tau}^2 + \bar{g}_{A\tau}^2} = -0.151 \pm 0.087\,.$$

Together with Γ_τ, the τ vector and axial-vector coupling constants have been determined as

$$\bar{g}_{V\tau} = -0.037 \pm 0.023$$

$$\bar{g}_{A\tau} = -0.494 \pm 0.008\,.$$

2.10 Leptonic vector and axial- vector couplings

Figures 20 and 21 show the measurements of the leptonic vector and axial-vector coupling constants, respectively. The coupling constants are determined from the leptonic Z widths, and the leptonic forward–backward asymmetries (and, in the ALEPH case, also from the charge asymmetry of hadronic jets, and the τ polarization). The measurements are in good agreement with each other, and with the MSM prediction. Note that the vector coupling constant, although small, is significantly different from zero.

The precision with which the leptonic vector and axial-vector coupling constants are known today is remarkable. Figure 22 from Ref. [13], recalls the experimental knowledge back in 1986. The results then stemmed from neutrino–electron scattering, polarized electron–deuteron scattering, polarized muon–carbon scattering, and $e^+e^- \to l^+l^-$ annihilation as measured at PEP and PETRA. With the advent of the LEP data, the errors have shrunk to such an extent that quite some magnification is needed in order to display the status as of today.

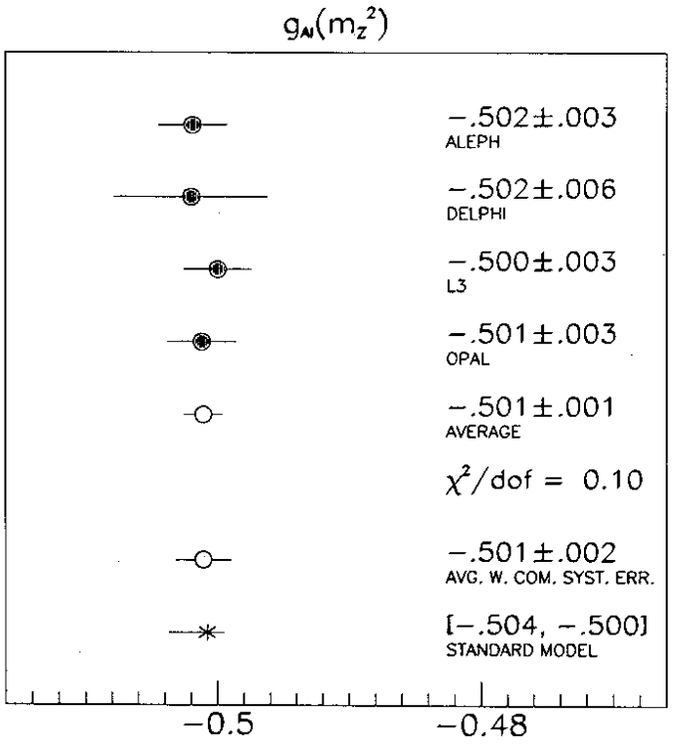

Figure 21: The leptonic axial-vector coupling constant

2.11 $\sin^2\bar{\theta}_{\rm w}$

The same measurements, which served for determining the leptonic vector and axial-vector coupling constants, also serve for determining the electroweak mixing parameter,

$$\sin^2\bar{\theta}_{\rm w} = 1 - \frac{m_W^2}{\bar{\rho} m_Z^2}\,.$$

For example, the leptonic Z width reads in terms of $\sin^2\bar{\theta}_{\rm w}$ as

$$\Gamma_l = \frac{\bar{\alpha} m_Z}{12\sin^2\bar{\theta}_{\rm w}\cos^2\bar{\theta}_{\rm w}}\left\{\left(\frac{1}{2} - 2\sin^2\bar{\theta}_{\rm w}\right)^2 + \left(\frac{1}{2}\right)^2\right\}.$$

Notice that the electroweak mixing parameter, if determined this way, has a knowledge about m_t and m_H incorporated in it. Because of that, the numerical value of $\sin^2\bar{\theta}_{\rm w}$ will stand whatever values m_t and m_H eventually take.

Figure 23 displays the measurements of $\sin^2\bar{\theta}_{\rm w}$ from the LEP experiments [12, 14, 15, 16]. The common systematic error is estimated at ± 0.0014, arising from a propagation of the theoretical uncertainty of the Bhabha cross-section. Without improvement in this sector, it will be hard to reduce the overall error on $\sin^2\bar{\theta}_{\rm w}$. The ultimate error on $\sin^2\bar{\theta}_{\rm w}$ is, without beam polarization, expected to be 0.001.

The value of the electroweak mixing parameter from LEP,

$$\sin^2\bar{\theta}_{\rm w} = 0.2301 \pm 0.0020\,,$$

constitutes the most precise determination so far, surpassing now the precision from the neutral-to-charged current ratio as measured in neutrino–nucleon scattering, and from the W and Z masses.

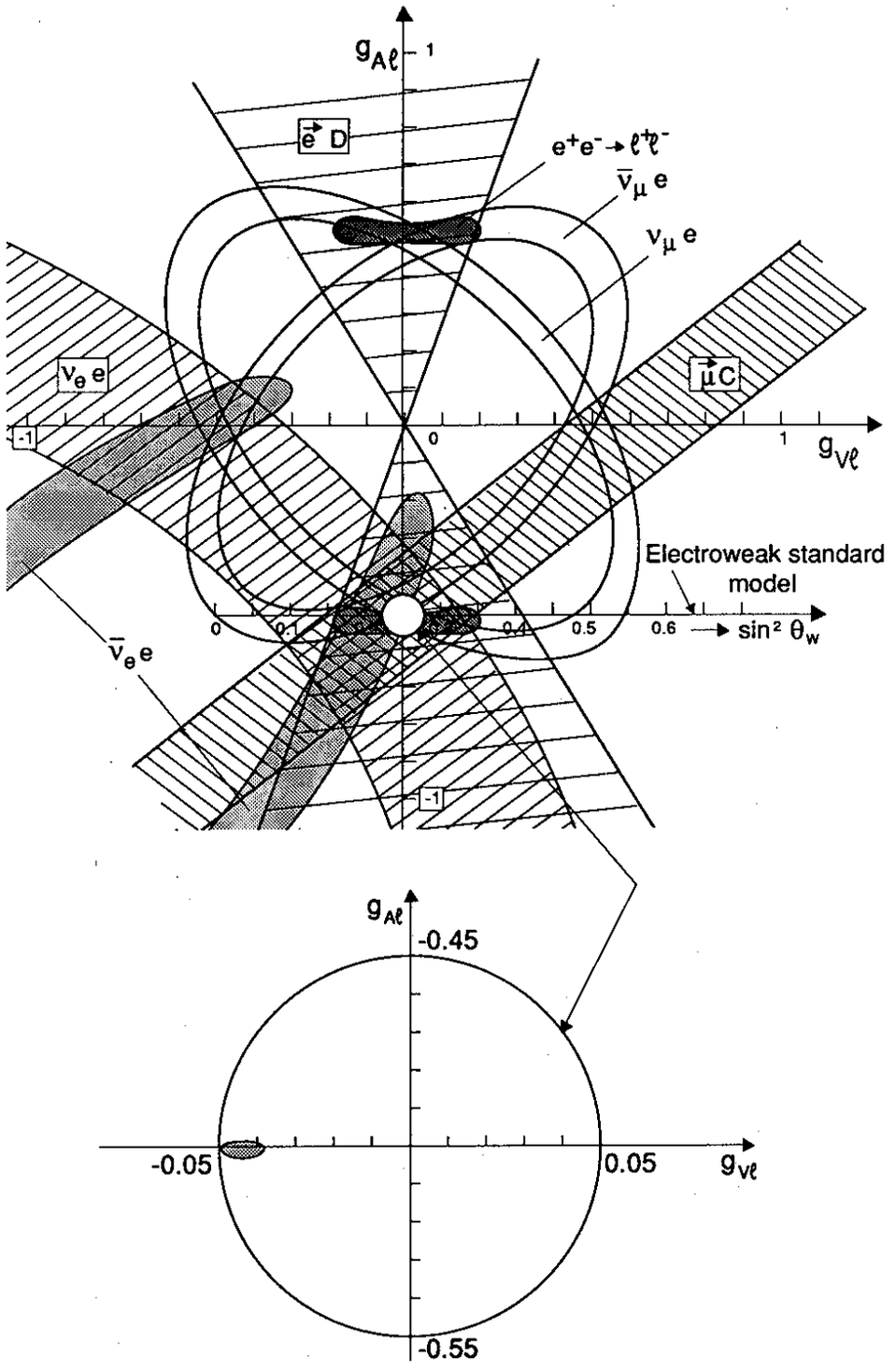

Figure 22: The knowledge of $\bar{g}_{Vl}$ and $\bar{g}_{Al}$ from various experiments, in 1986 and today

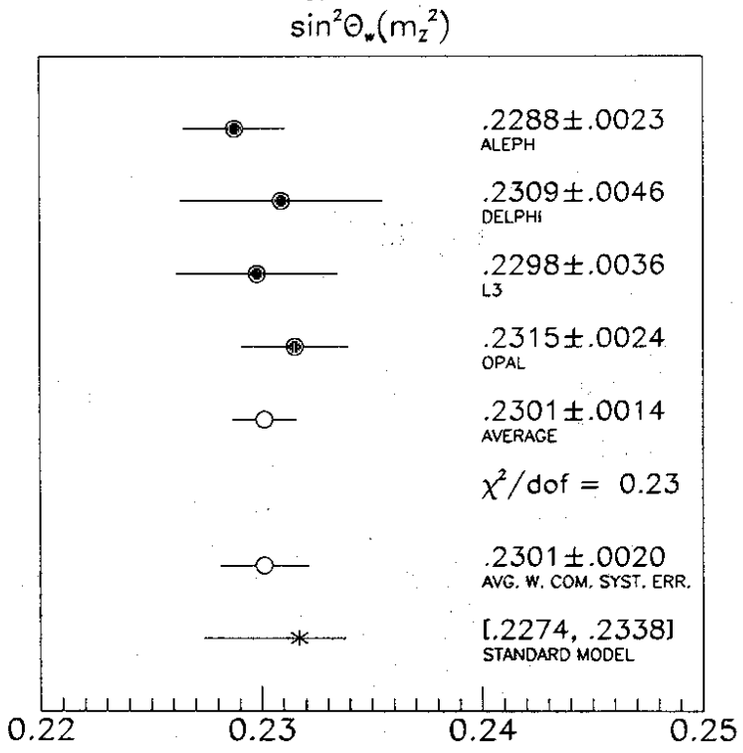

Figure 23: Measurements of $\sin^2\bar{\theta}_w$

As pointed out above, the value of $\sin^2\bar{\theta}_w$ determined from Γ_l is independent of m_t, in contrast with determinations of $\sin^2\bar{\theta}_w$ from the ratio m_W/m_Z in the $p\bar{p}$ collider experiments [17, 18], and, equivalently, the neutral-to-charged current ratio in neutrino–nucleon scattering experiments [19, 20], and from the Z mass. The question of which value of m_t makes all these measurements consistent is answered in Fig. 24. A fit to the experimental data yields the result [21]

$$\begin{aligned} m_t &= 139 \pm 32\,(\text{stat.}) \pm 20\,(m_H)\ \text{GeV} \\ &= 139 \pm 38\ \text{GeV}\,, \end{aligned}$$

where m_H is allowed to vary in the range from 40 to 1000 GeV. That constitutes today the best guess which we have about the mass of the t quark. Minor improvements to this analysis can be made if other data on electroweak processes are also taken into account [22].

With the best fit value of m_t, the W mass is then predicted to be

$$m_W = 80.17 \pm 0.25\ \text{GeV}\,,$$

quite consistent with the less precise experimental determinations [23].

2.12 Hadronic Z decay widths

The focus of attention was so far the determination of Γ_b, the width for the Z decay into b quarks. ALEPH, L3, and OPAL used b tagging via high-momentum and high-p_T leptons from semileptonic b decays. In contrast, DELPHI employed the concept of the 'boosted sphericity product', making use of the greater sphericity of b jets as compared to jets which originate from light quarks.

Table 3 lists the results obtained for $\mathrm{BR}(b \to l\nu X)\Gamma_b/\Gamma_h$ and for Γ_b/Γ_h. The results are in good agreement. In view of the rather large uncertainty on the effective semileptonic branching

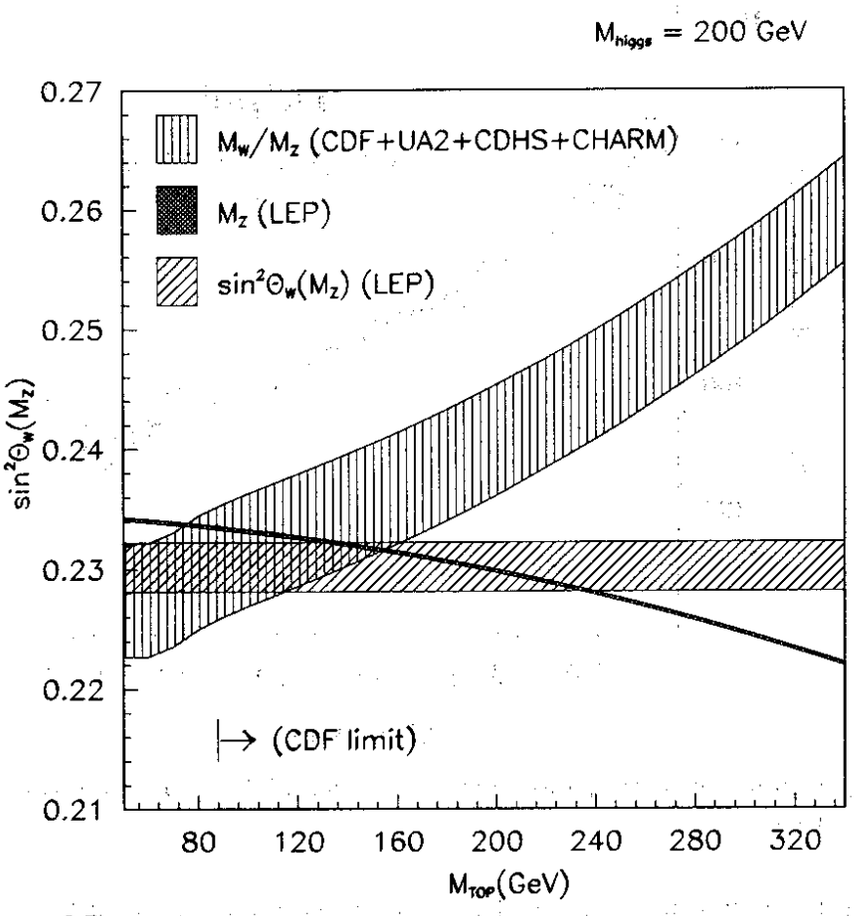

Figure 24: $\sin^2 \bar{\theta}_{\rm w}$ as a function of m_t, for $m_H = 200$ GeV, from various experiments

Table 3: Results on the Z width for the decay into b quarks

	Method	$BR(b \to l\nu X)\Gamma_b/\Gamma_h$	Γ_b/Γ_h
ALEPH [8]	e, μ	0.0224 ± 0.0019	
DELPHI [24]	S_1*S_2		0.209 ± 0.043
L3 [25]	μ	0.0248 ± 0.0014	
MARK II [26]	e, μ	0.0250 ± 0.0110	
OPAL [10]	μ	0.0206 ± 0.0021	
Average		0.0232 ± 0.0010	

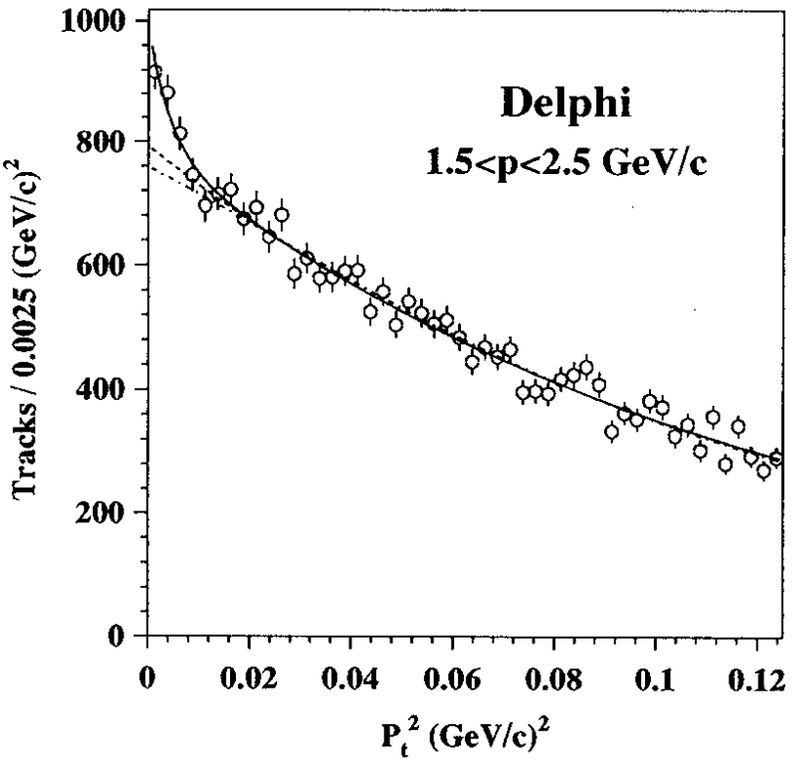

Figure 25: p_T^2 spectrum of charged pions, showing a signal of $D^* \to D^0\pi$ decays at low momentum and low p_T^2 (DELPHI)

Table 4: Results for the width of the Z decay into charmed hadrons

	Method	Γ_c (MeV)
ALEPH [8]	electrons	260 ± 110
DELPHI [27]	low-p_t pions	282 ± 103
L3 [25]	muons	221 ± 45

ratio BR($b \to l\nu X$) we prefer, rather than to quote a value of Γ_b, to utilize the MSM prediction, $\Gamma_b/\Gamma_h = 0.217$, to deduce the effective semileptonic branching ratio of the b quark, at the Z pole,

$$\mathrm{BR}(b \to l\nu X) = 0.107 \pm 0.005\,,$$

a value which is consistent with expectations.

The tagging of $Z \to c\bar{c}$ decays has been performed with high-momentum and medium-p_T leptons from semileptonic c quark decay, by ALEPH and L3. DELPHI have employed the tagging through very low-p_T pions stemming from the decay $D^* \to D^0\pi$ (see Fig. 25). Table 4 lists the results obtained for the charmed Z width, Γ_c. The results are in agreement with each other, and with the MSM prediction, but are not yet precise.

2.13 Decay width into up-like and down-like quarks

OPAL [16] have measured the ratio of hadronic events with single, isolated, photons, to the total number of hadronic events. By selecting events where the photon is radiated off the final-state quarks, the above ratio measures the square of the electric charge of the final-state quarks. The

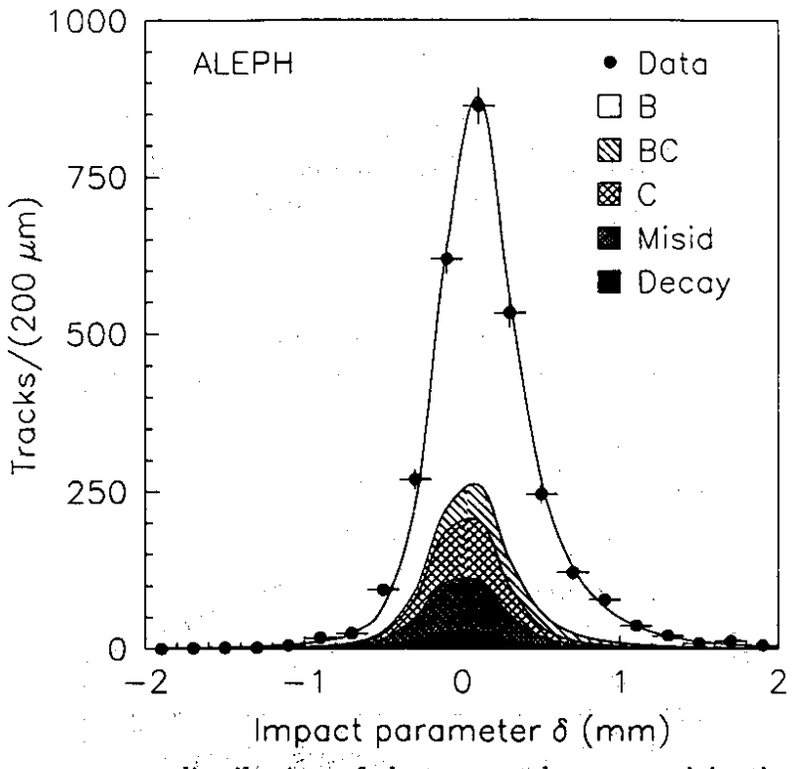

Figure 26: Impact-parameter distribution of electrons and muons originating from semileptonic b decays (ALEPH)

measured widths $\Gamma(Z \to q\bar{q}\gamma)$ and Γ_h are interpreted in terms of the sum of the squares of up-like and down-like vector and axial-vector coupling constants. This yields the Z decay widths

$$\Gamma(Z \to u\bar{u}) = 330 \pm 99 \text{ MeV}$$

$$\Gamma(Z \to d\bar{d}) = 369 \pm 67 \text{ MeV} ,$$

in agreement with the MSM predictions of 378 and 299 MeV, respectively.

2.14 Average B lifetime

ALEPH presented a measurement [28] of the average lifetime of b flavoured hadrons, derived from the distribution of the impact parameters of high-momentum, high-p_T electrons and muons. The impact parameter is defined with respect to the colliding-beam centre.

As can be seen from Fig. 26, the impact parameter distribution has a significant non-zero average, amounting to 140 μm, which corresponds to an average B lifetime of

$$\langle \tau_B \rangle = (1.28 \pm 0.14) \times 10^{-12} \text{s} ,$$

which is in good agreement with the current world average,

$$\langle \tau_B \rangle = (1.13 \pm 0.15) \times 10^{-12} \text{s} .$$

2.15 $B^0\bar{B}^0$ mixing

ALEPH and L3 analysed their high-momentum, high-p_T samples of dileptons ($ee, e\mu$, and $\mu\mu$) with a view to observing an 'abnormal' ratio of like-sign to opposite-sign lepton pairs, signalling $B^0\bar{B}^0$ mixing.

Table 5: Results for the B mixing parameter χ

	Method	χ
ALEPH [8]	ee, eμ, $\mu\mu$	0.129 ± 0.046
L3 [29]	$\mu\mu$	$0.178^{+0.049}_{-0.040}$

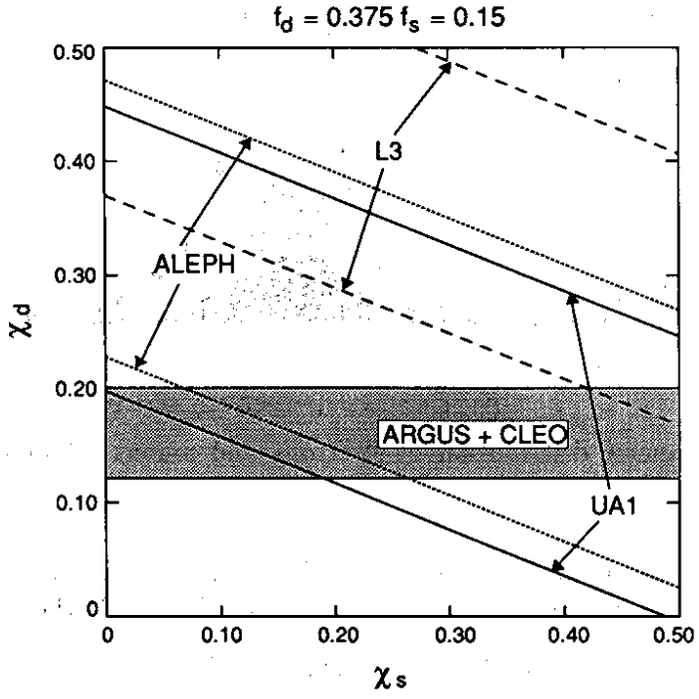

Figure 27: Allowed domains for the B mixing parameters χ_d and χ_s

The results for the mixing parameter χ, which denotes the probability of a B turning into a $\bar{B}$ during its lifetime, are given in Table 5. The thus-measured mixing parameter is a superposition of B_d and B_s mixing: $\chi = f_d\chi_d + f_s\chi_s$, with f_d and f_s denoting the relative weights, estimated from Monte Carlo simulations of the hadronization of the b quark. Figure 27 shows the current status of affairs, assuming 'reasonable' numerical values of $f_d = 0.375$ and $f_s = 0.15$. The results from LEP are in good agreement with other results from UA1 [30], ARGUS [31] and CLEO [32], but are not yet good enough to give unambiguous evidence of B_s mixing – one of the areas where more data are eagerly awaited.

3 QCD

For an in-depth review of recent QCD results, with emphasis on the theoretical issues, we refer to the talk given by M. Jacob at this conference. Here, we restrict ourselves to a brief review of the measurements of the strong coupling constant in hadronic Z decays.

The process of quark creation and hadronization in Z decays is depicted in Fig. 28. The first phase, the electroweak creation of a quark pair at $Q^2 = m_Z^2$, is well understood. The second phase, gluon radiation and gluon splitting at the same large Q^2, is considered well described by perturbative QCD. In practice, two approaches have been employed in the frame of Monte Carlo

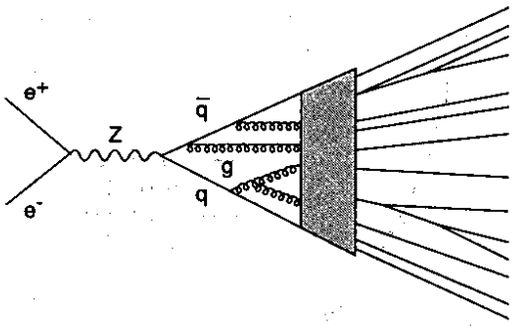

Figure 28: Creation and hadronization of quarks in hadronic Z decays

simulations:

- the 'ME' approach, involving matrix elements calculated to $\mathcal{O}(\alpha_s^2)$ inclusive [33], and
- the 'LLA' approach, a leading-logarithm approximation [34].

In the third phase, the hadronization of quarks and gluons takes place at $Q^2 \simeq 1$ GeV^2. As there is no theory of hadronization, a variety of more or less QCD-inspired models have been proposed which are available in the form of Monte Carlo generators:

- independent hadronization models [35], which are known not to describe the data adequately unless some *ad hoc* cures are applied (such as proposed in Ref. [36]),
- string hadronization [37],
- cluster hadronization [38], and
- string hadronization with colour coherence [39].

Of these, string hadronization with colour coherence compares perhaps most favourably with the data.

In much the same way as in the sector of electroweak radiative corrections, we are greatly indebted to the many authors [40] who developed models of all three phases of quark creation and subsequent hadronization, and made them available in the form of Monte Carlo generators. Without their work, the many results on QCD from hadronic Z decays would have been impossible.

In the first round of QCD studies in hadronic Z decays, the emphasis was on a comparison of the ME formulation with the LLA formulation of the perturbative phase. Out of many distributions which have been presented by the experiments, Fig. 29 may be representative. It shows the aplanarity distribution of hadronic Z decays as measured by OPAL, in comparison with the ME and LLA predictions as incorporated in the Monte Carlo generators JETSET 7.2, HERWIG 3.4, and ARIADNE 3.1. From this and other comparisons the conclusion emerges that the LLA approach permits a better representation of the data, presumably because the ME approach is limited to a maximum of four final-state partons, and hence constitutes an inadequate representation of the gluon activity. This is particularly visible in variables such as aplanarity and p_T^{out}, which are sensitive to the activity perpendicular to the qqg plane. In contrast, the LLA approach has no such *a priori* limitation on the number of partons.

In view of this shortcoming of the ME approach, a 'remedy' for the missing higher orders has been introduced: in order to enhance the gluon activity, a larger value of α_s is being used by utilizing a smaller Q^2 scale, $\mu^2 = fQ^2$, where f is an empirically determined factor. This change of Q^2 scale is a measure of the missing higher orders in the perturbation expansion.

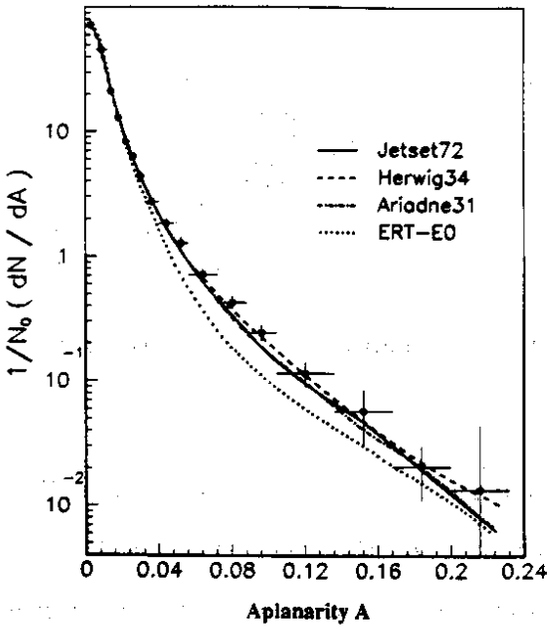

Figure 29: Aplanarity distribution of hadronic Z decays: data and comparison with the ME and LLA formulation (OPAL)

In contrast to the LLA approach, the ME approach has a well-defined Q^2 scale, which is needed for a measurement of α_s. As a satisfactory measurement requires good agreement with the data, a change of the Q^2 scale to smaller values seems inescapable for the time being until higher orders are included in the theoretical predictions.

So far, two methods have been employed for determining $\alpha_s(m_Z^2)$:

- *Jet multiplicity*

  The commonly adopted algorithm for determining the number of jets in a hadronic event is the 'JADE' algorithm: all pairs of hadrons and partons, respectively, are iteratively merged until

  $$y_{ij} = \frac{2E_i E_j(1-\cos\Theta_{ij})}{E_{vis}^2}$$

  is larger than a given cut-off value y_{cut} for any pair (i,j) of hadrons and partons, respectively. This leads, as a function of y_{cut}, to a well-defined jet multiplicity, which in turn determines $\alpha_s(m_Z^2)$. Monte Carlo studies at the parton and hadron levels have shown that little bias is introduced in the transition from partons to hadrons. The largest systematic uncertainty arises from the unknown Q^2 scale. Until calculations at $\mathcal{O}(\alpha_s^3)$ become available it is recommended that results are evaluated not only on the Q^2 scale m_Z^2, but also on $(m_Z/2)^2$ and $(m_Z/4)^2$.

  Figure 30 shows, as an example, the L3 data on the jet multiplicity as a function of y_{cut}. Whilst the data on the two- and three-jet fractions are well reproduced by the Monte Carlo, there are, not surprisingly, some difficulties with the fraction of four or more jets.

  Figure 31 shows the measurements of $\alpha_s(m_Z^2)$ from the four LEP Collaborations. The overall experimental error is dominated by the common systematic error due to the theoretical uncertainty of the Q^2 scale, and, to a lesser extent, of the hadronization mechanism. Further progress depends on a better understanding of the theory.

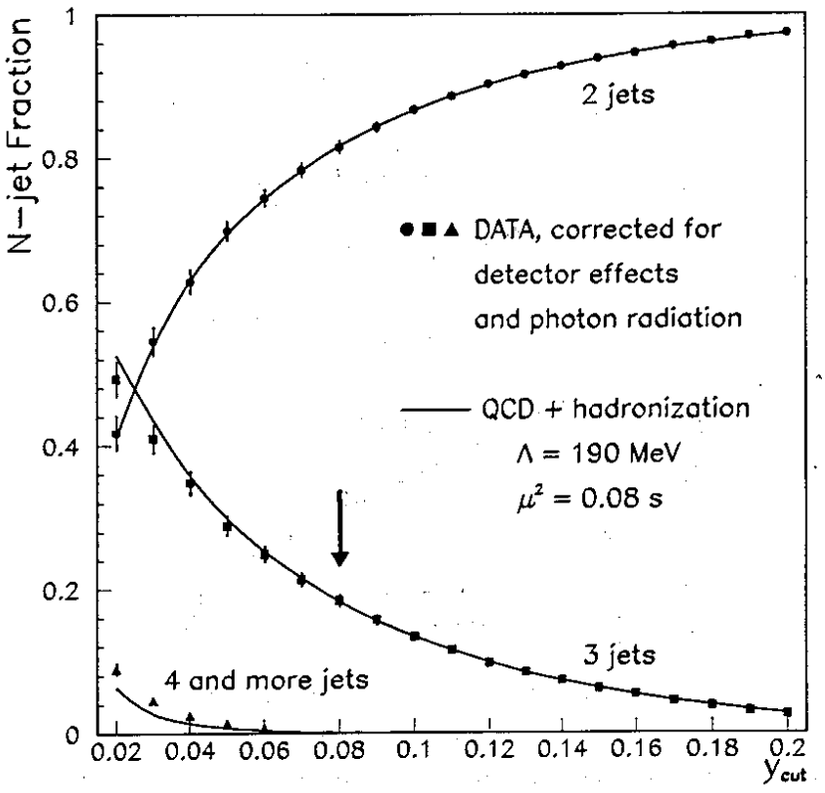

Figure 30: Fraction of two-, three- and four-jet events, as a function of $y_{\rm cut}$ (L3)

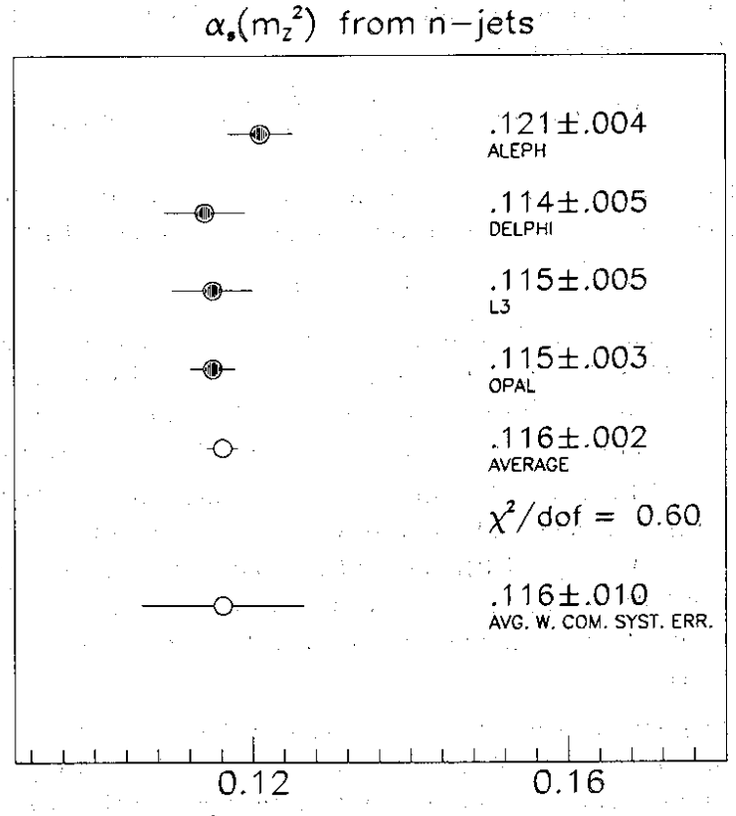

Figure 31: $\alpha_s(m_Z^2)$ as determined from the jet multiplicity

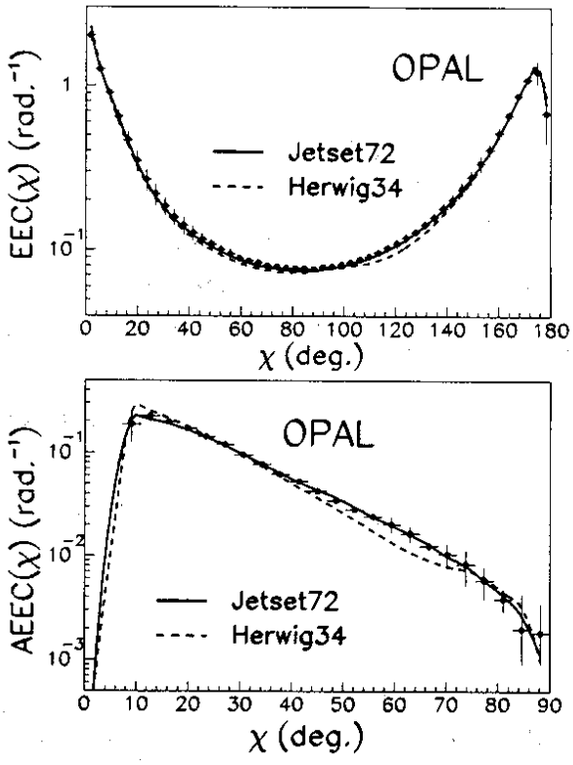

Figure 32: Energy–energy correlation, and asymmetric energy–energy correlation (OPAL)

- *Energy–energy correlations*

  Let χ_{ij} denote the angle between hadrons i and j of a hadronic event. The energy–energy correlation (EEC) is then defined as

$$\mathrm{EEC}(\cos\chi) = \frac{1}{N} \sum_{\text{events}} \sum_{\text{i,j}} \frac{E_i E_j}{E_{\text{vis}}^2} \delta(\cos\chi - cos\chi_{ij}) \,.$$

  Two methods have been employed for reducing the uncertainty due to the transition from partons to hadrons: the asymmetric energy–energy correlation (AEEC),

$$\mathrm{AEEC}(\cos\chi) = \mathrm{EEC}[\cos(\pi - \chi)] - \mathrm{EEC}(\cos\chi) \,,$$

  which has still a fair bias from the transition from partons to hadrons, and the cluster energy–energy correlation (CEEC), which has been proposed by ALEPH. In the latter method, the hadrons are first merged into clusters before looking at their energy–energy correlation. Their claim is that there is only a small bias from the parton to hadron transition.

  Figure 32 shows the EEC and AEEC distributions as measured by OPAL, together with the best fits of predictions of shower Monte Carlo models. Figure 33 shows the best values of α_s as determined from CEEC (ALEPH) and AEEC (DELPHI, L3, and OPAL). The common systematic error of 0.01 due to the hadronization mechanism and, to a lesser extent, due to the Q^2 scale, is retained, and a similar remark about further progress applies as is made above for the jet multiplicity.

Does α_s 'run'? This long-standing question is answered in Fig. 34. Various determinations of the 3-jet fraction (which measures α_s) from the reaction $e^+e^- \rightarrow$ hadrons are plotted against $\sqrt{s}$ [41]. One can put forward many arguments as to the systematic errors of the procedures that have been utilized to determine α_s; however we cannot escape the conclusion that α_s does 'run' much in the way required by perturbative QCD.

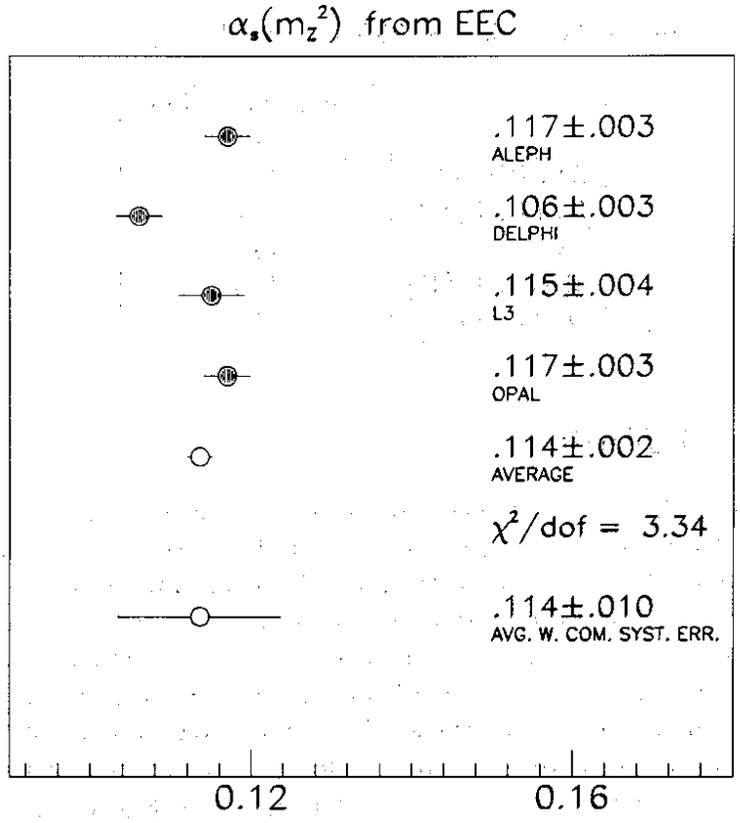

Figure 33: $\alpha_s(m_Z^2)$ as determined from energy–energy correlations

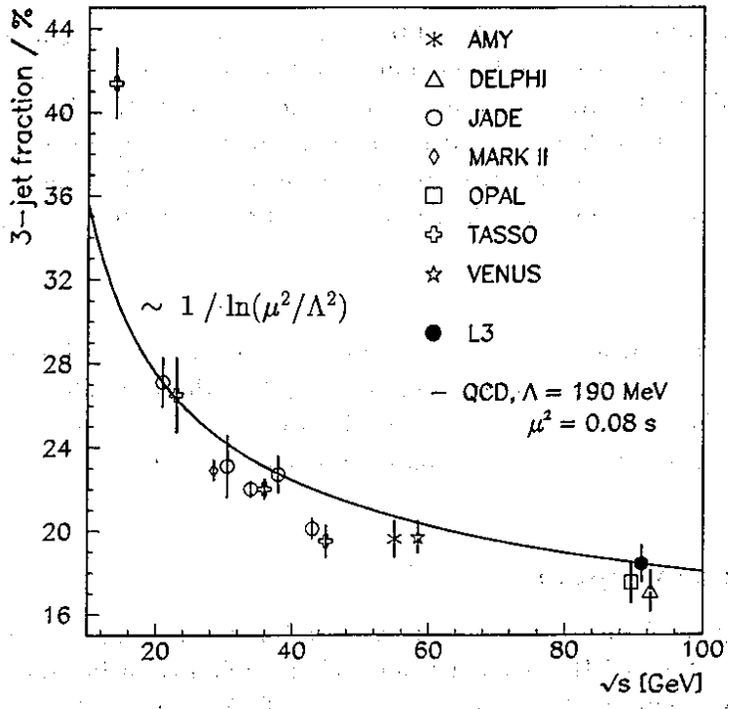

Figure 34: Compilation of 3-jet fractions as measured in e^+e^- → hadrons at various energies (compiled by L3)

Table 6: Lower limits (95% CL) on the t quark mass

	t quark mass limit (GeV)
ALEPH [42]	45.8
DELPHI [43]	44.0
L3 [44]	46.0
MARK II [45]	40.7
OPAL [46]	45.1

4 Searches and Limits

According to our belief that all constituents of matter – known or unknown – participate in the weak interaction, Z decays are an ideal laboratory for the search for new particles through their weak coupling to the Z. On the basis of their predicted production cross-section, corrected for initial-state bremsstrahlung, and the known luminosity, sensitive searches for the existence of such particles can be made. In most of the cases the production cross-section is so large that the search is kinematically limited, i.e. by the available beam energy. In other cases, notably in that of the standard Higgs, the search is limited by the available integrated luminosity.

No new particle has been discovered so far in Z decays. For the time being, the results comprise mostly lower limits on the masses of expected or hypothetical heavy new particles.

4.1 t quark

The Z decay into a pair of t quarks would lead to a rather spherical event shape, largely independent of the specific decay mode and hence independent of the assumption of a semileptonic branching ratio just as predicted by the MSM (the limit $m_t > 89$ GeV at 95% CL put forward by the CDF Collaboration [47] relies on such a 'standard' semileptonic branching ratio). The searches at LEP and at the SLC, however, are also sensitive to decays such as $t \to bW^*$ and $t \to bH^+$. Table 6 lists the lower mass limits for the t quark. The search is limited by the beam energy.

4.2 b' quark

The direct search for the down-like quark of a possible massive fourth family through a spherical event shape, which is sensitive to standard and non-standard decay modes such as $b' \to cW^*$, cH^-, bg, and $b\gamma$, leads to the lower mass limits listed in Table 7. The search is limited by the beam energy. The confirmed absence of the b' quark is consistent with what has been inferred from neutrino counting.

4.3 Sequential heavy lepton $L^\pm$

A sequential heavy lepton $L^\pm$ is expected to decay into its own associated neutrino ν_L and a virtual W: $L^\pm \to \nu_L \mathrm{W}^*$. Whilst ALEPH excluded from their neutrino counting result an $L^\pm$ of *any* mass provided the associated neutrino has a mass $m_{\nu_L} < 42.7$ GeV at 95% CL, L3 and OPAL performed in addition direct searches by looking for isolated leptons with associated missing energy. The lower mass limits are listed in Table 8. The search is limited by the beam energy.

Table 7: Lower limits (95% CL) on the b' quark mass

	b' quark mass limit (GeV)
ALEPH [42]	46.0
DELPHI [43]	44.5
L3 [44]	46.0
MARK II [45]	44.7
OPAL [46]	45.4

Table 8: Lower limits (95% CL) on the mass of the sequential heavy lepton $L^{\pm}$

	$L^{\pm}$ mass limit (GeV)
ALEPH [42]	m_{Planck} if $m_{\nu_L} < 42.7$
L3 [44]	43.9
OPAL [46]	44.3

4.4 Neutral stable heavy lepton L^0

A neutral stable heavy lepton is a neutrino-like particle. ALEPH and L3 interpreted their results on neutrino counting in terms of a mass limit on a Dirac neutrino of a fourth family. Table 9 lists their lower mass limits. The lower limit of 42.8 GeV from L3 for a Dirac neutrino would transform into a lower limit of 34.8 GeV (95% CL) for a Majorana neutrino. The search is limited by the beam energy.

4.5 Neutral unstable heavy lepton L^0

A neutral unstable heavy lepton L^0 would be a superposition of the three known neutrino states,

$$L^0 = \sum_l U_{Ll}\nu_l \ \ (l = e, \mu, \tau)\,,$$

with a decay $L^0 \to lW^*$. The signature would be isolated high-momentum leptons in a direct search, and modifications of the measured total and hadronic Z widths in an indirect search. Table 10 lists the lower mass limits. The search is limited by the beam energy.

Table 9: Lower limits (95% CL) on a neutral stable heavy lepton L^0

	L^0 mass limit (GeV)
ALEPH [42]	42.7
L3 [48]	42.8

Table 10: Lower limits (95% CL) on a neutral unstable heavy lepton L^0

	L^0 mass limit (GeV)
ALEPH [42]	42.7
L3 [48]	46.4
OPAL [46]	45.7

Table 11: Lower limits (95% CL) on excited charged leptons $l^{*\pm}$, for $\lambda = 1$ (the upper rows refer to pair production, the lower rows to single production)

	Mass limits		
	$e^{*\pm}$ (GeV)	$\mu^{*\pm}$ (GeV)	$\tau^{*\pm}$ (GeV)
ALEPH [42]	45.6	45.6	45.4
	89.0	89.0	89.0
L3 [49]	45.0	45.3	45.5
	88.0	85.0	89.0
OPAL [46]	44.9	44.9	44.9
	87.0	86.0	83.0

4.6 Excited charged lepton $l^{*\pm}$

An excited charged heavy lepton would decay radiatively into a normal charged lepton: $l^{*\pm} \to l^{\pm}\gamma$, with an isolated high-energy photon as signature. The mass limits are naturally depending on whether a l^*l^* or l^*l pair is produced. The non-observation of such events leads to an excluded domain when the mass of the excited lepton, $m_{l^*\pm}$, is plotted against the Zl^*l^* coupling strength, $\lambda/m_{l^*\pm}$. Table 11 lists the mass limits obtained for the specific case $\lambda = 1$. The search is more limited by the beam energy than by the integrated luminosity.

4.7 Excited neutrino ν^*

ALEPH [50] searched for excited neutrinos via the radiative decay $\nu^* \to \nu\gamma$. The signature would be one or two high-energy photons, depending on whether a single excited neutrino or a pair has been created. The decay $Z \to \nu^*\bar{\nu}^*$ is excluded for $\mathrm{BR}(Z \to \nu^*\bar{\nu}^*) \times \mathrm{BR}^2(\nu^* \to \nu\gamma) > 7{\times}10^{-5}$ at 95% CL, whereas the decay $Z \to \nu^*\nu$ is excluded for $\mathrm{BR}(Z \to \nu^*\nu) \times \mathrm{BR}(\nu^* \to \nu\gamma) > 6{\times}10^{-5}$ at 95% CL. L3 [51] reported comparable limits from a search for both decay modes $\nu^* \to \nu\gamma$ and $\nu^* \to eW^*$. The search is limited by the integrated luminosity.

4.8 MSM neutral Higgs boson H^0

A considerable effort has gone into the search for the neutral Higgs boson which is required by the MSM. The search was performed through the decay $Z \to H^0Z^*$, with $Z^* \to e^+e^-, \mu^+\mu^-$, and $\nu\bar{\nu}$. Emphasis was put on excluding a light H^0 down to zero mass, in order to close a window which was affected by uncertainties as to the reliability of the theoretical predictions of rare meson decays involving the H^0.

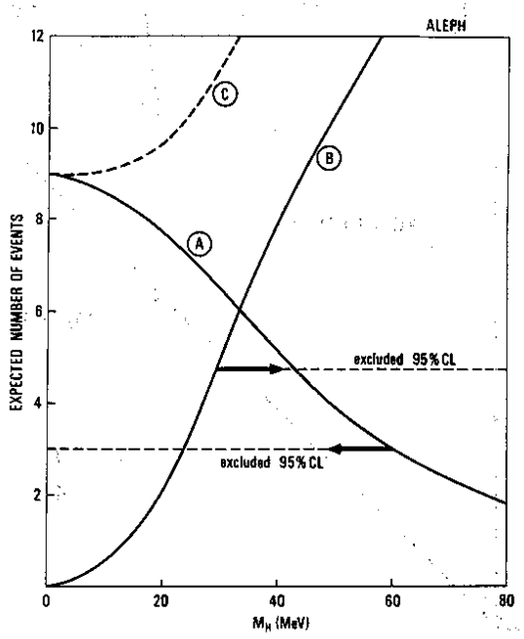

Figure 35: Number of events expected for a low-mass H^0. Curve A refers to an undetected H^0, curve B to a H^0 which decays after a finite path length into an e^+e^- pair (ALEPH)

Table 12: Mass range of the MSM H^0 excluded at 95% CL

	Excluded MSM H^0 mass (GeV)
ALEPH [52, 56]	$0 \leq m_H \leq 41.6$
DELPHI [53]	$0 \leq m_H \leq 34.0$
L3 [54, 57]	$0 \leq m_H \leq 41.4$
OPAL [55, 58]	$0 \leq m_H \leq 0.21$
	$3 \leq m_H \leq 44.0$

For a very low-mass H^0 ($m_H < 2m_e$), the particle tends to leave the apparatus undetected as its lifetime becomes large. Figure 35 shows the number of events in ALEPH [52], for an undetected low-mass H^0 as a function of its mass. The decrease in efficiency towards larger H^0 mass is compensated by the search for events where the H^0 decays, after a finite path length, still inside the apparatus into an e^+e^- pair. Both searches together exclude a low-mass H^0 to more than 95% CL. Analogous conclusions have been drawn by DELPHI [53], L3 [54], and OPAL [55].

The search for a heavy H^0 is limited by the integrated luminosity, since the cross-section for $Z \to H^0 Z^*$ is steeply falling with increasing m_H. The signature is an e^+e^-, $\mu^+\mu^-$, or $\nu\bar{\nu}$ pair from Z^* decay, together with the decay products of the heavy H^0, mostly $b\bar{b}$. The cuts are carefully optimized so as to extend the sensitivity to the highest masses while keeping the background negligible. The mass range excluded by the LEP experiments is given in Table 12. Because of the limitation coming from the available integrated luminosity it is tempting to combine the results from the four experiments and thus obtain an even better lower limit on m_H. However, such a procedure would be unsafe: the experimental cuts are such that the efficiency of the search falls rapidly above the limits quoted by each experiment, and background shows up. A combination of the results would thus require a more detailed study.

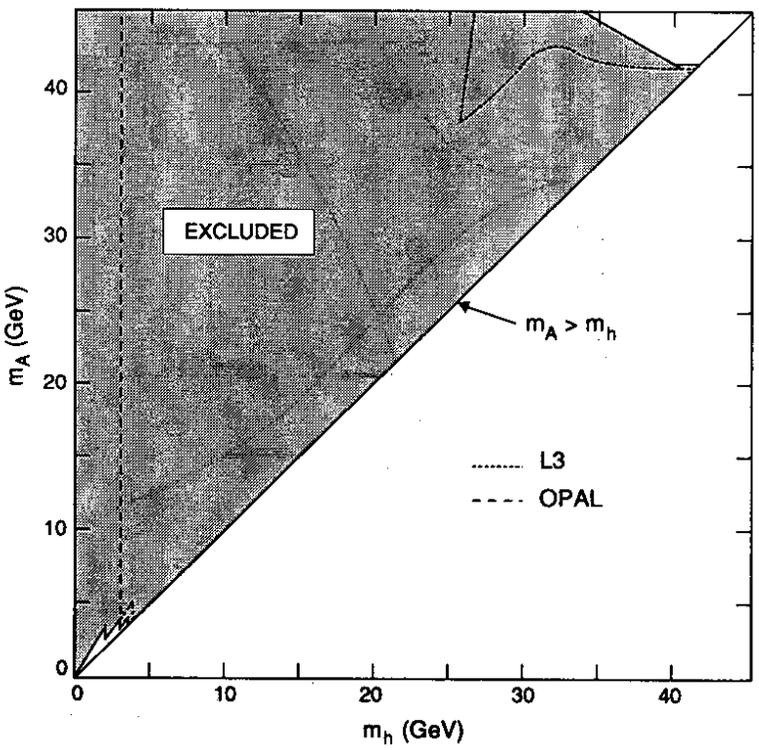

Figure 36: Excluded domain (95% CL) in m_h vs m_A, for $v_2/v_1 > 1$

4.9 MSSM neutral Higgs bosons h, A

In the minimal supersymmetric extension of the Standard Model (MSSM), the following superpartners of the vector mesons γ, Z, and W, and of the five physical Higgs bosons h, A, H^0, and $H^\pm$, which constitute the minimal Higgs content of the MSSM, should exist:

$W^\pm, H^\pm \Longleftrightarrow \tilde{W}_1^\pm, \tilde{W}_2^\pm$ (winos)
$\gamma \Longleftrightarrow \tilde{\gamma}$ (photino)
$Z, H^0 \Longleftrightarrow \tilde{Z}_1, \tilde{Z}_2$ (zinos)
$h, A \Longleftrightarrow \tilde{H}$ (higgsino)

The two winos will in general mix, resulting in two charginos, $\tilde{\chi}_1^\pm, \tilde{\chi}_2^\pm$. The photino, the two zinos and the higgsino will in general mix, resulting in four neutralinos $\tilde{\chi}_i^0$ (i = 1...4). For the Higgs content of the MSSM, the following hierarchy in the masses is predicted [59]: $m_h < m_Z$ and $m_A > m_h$.

There are two independent parameters in the MSSM which are taken as m_A and m_h.

Figure 36 shows the domain in m_h and m_A which has been excluded by the LEP experiments [60, 46]. The limit $m_A > m_h > 32$ GeV (95% CL) holds, if $v_2/v_1 > 1$ as is theoretically favoured. The search is limited by the integrated luminosity.

4.10 Charged Higgs boson $H^\pm$

The charged Higgs boson decays into heavy fermion pairs: $H^+ \to \nu\bar{\tau}, c\bar{s}$, and $c\bar{b}$, with branching ratios which are not fixed within the MSSM. For the assumption BR($H^+ \to \nu\bar{\tau}$) = 50%, Table 13 lists the lower mass limits obtained by the experiments. The search is limited by the beam energy.

Table 13: Lower limits (95% CL) for the charged Higgs boson $H^{\pm}$, assuming BR($H^+ \to \nu\bar{\tau}$) = 50%

	$H^{\pm}$ mass limit (GeV)
ALEPH [42]	40.6
DELPHI [53]	42.0
L3 [61]	40.7
OPAL [62]	41.5

Table 14: Lower limits (95% CL) for the squarks $\tilde{u}$ and $\tilde{d}$

	$\tilde{u}$ mass limit (GeV)	$\tilde{d}$ mass limit (GeV)
DELPHI [43]	42.0	43.0
L3 [44]	45.4	45.4
MARK II [63]	40.0	42.0

4.11 Sneutrino $\tilde{\nu}$

The L3 Collaboration [44] have determined a lower limit for the sneutrino mass, from their result on neutrino counting: $m_{\tilde{\nu}} > 31.9$ GeV (95% CL). The search is beam energy limited.

4.12 Squarks $\tilde{u}$ and $\tilde{d}$

The squarks $\tilde{u}$ and $\tilde{d}$ were searched for through their decays $\tilde{u} \to u\tilde{g}$ and $\tilde{d} \to d\tilde{g}$, respectively. Table 14 lists the lower mass limits obtained. The search is beam energy limited.

4.13 Selectron $\tilde{e}$, smuon $\tilde{\mu}$, and stau $\tilde{\tau}$

The charged sleptons $\tilde{l} = \tilde{e}, \tilde{\mu}$, and $\tilde{\tau}$ are assumed to decay by emission of the lightest neutralino, which escapes detection thus leading to acoplanar events: $\tilde{l} \to l\tilde{\chi}_1^0$. Table 15 lists the lower mass limits obtained under the assumption of left–right degeneracy, $m_{\tilde{l}_L} = m_{\tilde{l}_R}$, and $m_{\tilde{\chi}_1^0} \leq 10$ GeV. The searches are beam energy limited. Figure 37 shows, for example, the domain in $m_{\tilde{\tau}}$ and $m_{\tilde{\chi}_1^0}$ which has been excluded by DELPHI.

4.14 Chargino $\tilde{\chi}_1^{\pm}$

The lighter chargino $\tilde{\chi}_1^{\pm}$ has been searched for via its decay into the lightest neutralino and a virtual W: $\tilde{\chi}_1^{\pm} \to \tilde{\chi}_1^0 W^*$, leading to acoplanar fermion pairs from W^* decay. Table 16 lists the lower mass limits obtained under the assumptions that the lighter chargino is a wino-state (the limits are worse for a higgsino-state as the production cross-section is lower in that case), and that $m_{\tilde{\chi}_1^0} \leq 10$ GeV.

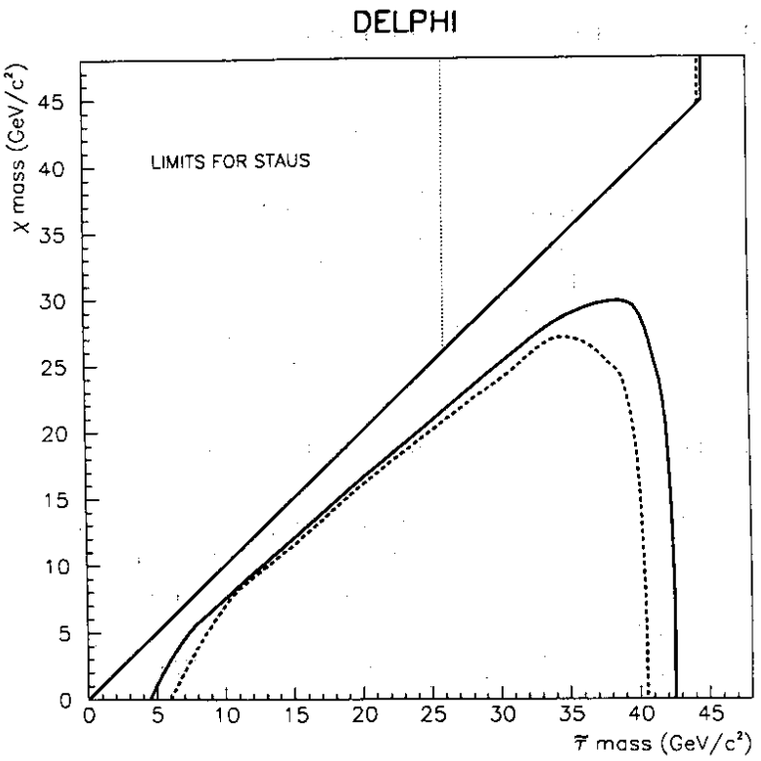

Figure 37: Excluded domain (95% CL) in $m_{\tilde{\tau}}$ and $m_{\tilde{\chi}_1^0}$ (DELPHI)

Table 15: Lower limits (95% CL) for the sleptons

	Mass limits		
	$\tilde{e}$ (GeV)	$\tilde{\mu}$ (GeV)	$\tilde{\tau}$ (GeV)
ALEPH [42]	43.5	42.6	40.4
DELPHI [43]	44.0	44.0	42.5
L3 [44]	41.0	44.0	
OPAL [46]	43.5	43.0	43.0

Table 16: Lower limits (95% CL) for the chargino $\tilde{\chi}_1^{\pm}$ (assuming a wino-state and $m_{\tilde{\chi}_1^0} \leq 10$ GeV)

	$\tilde{\chi}_1^{\pm}$ mass limit (GeV)
ALEPH [42]	44.5
DELPHI [43]	44.5
L3 [44]	44.0
MARK II [63]	43.0
OPAL [46]	45.0

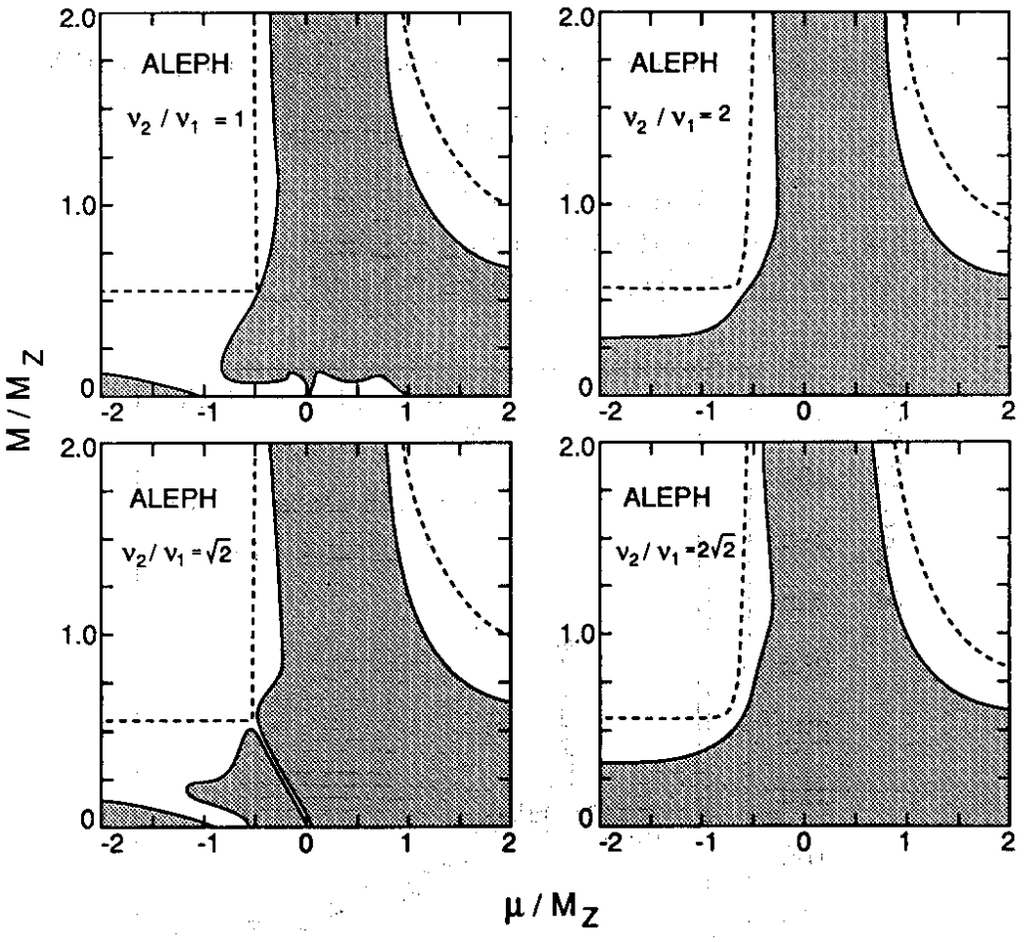

Figure 38: Excluded domains (95% CL; hatched areas) in the neutralino parameters m/m_Z and μ/m_Z, for four values of v_2/v_1 (ALEPH)

4.15 Neutralinos $\tilde{\chi}_1^0, \tilde{\chi}_2^0$

The lightest neutralinos have been searched for via the decays $\tilde{\chi}_2^0 \to \tilde{\chi}_1^0 Z^*, \tilde{\chi}_1^0 \gamma$, with the $\tilde{\chi}_1^0$ escaping detection. The negative results of the searches lead to excluded domains in a three-dimensional parameter space spanned by the ratios m/m_Z, and μ/m_Z, where m denotes the photino mass, μ the supersymmetric mass term which mixes the higgsino fields, and v_2/v_1 the expectation values of the Higgs doublet which is required in the framework of the MSSM. Figure 38 shows the result from ALEPH [42]. DELPHI [43], L3 [44], and OPAL [46] arrived at analogous conclusions. The values of v_2/v_1 in Fig. 38 are chosen so as to match current theoretical preferences.

4.16 Heavy stable charged particles

DELPHI, MARK II, and OPAL have performed a search for the pair production of heavy stable charged particles which would move slowly and would be recognized either by their low momentum, and/or by their enhanced ionization capability. Table 17 lists the mass ranges that have been excluded for such particles. The search is limited by the beam energy.

Table 17: Excluded mass range (95% CL) for heavy stable charged particles

	Excluded mass range (GeV)
DELPHI [64]	$25 \leq m \leq 45$
MARK II [65]	$0.21 \leq m \leq 36.3$
OPAL [66]	$18.5 \leq m \leq 42.8$

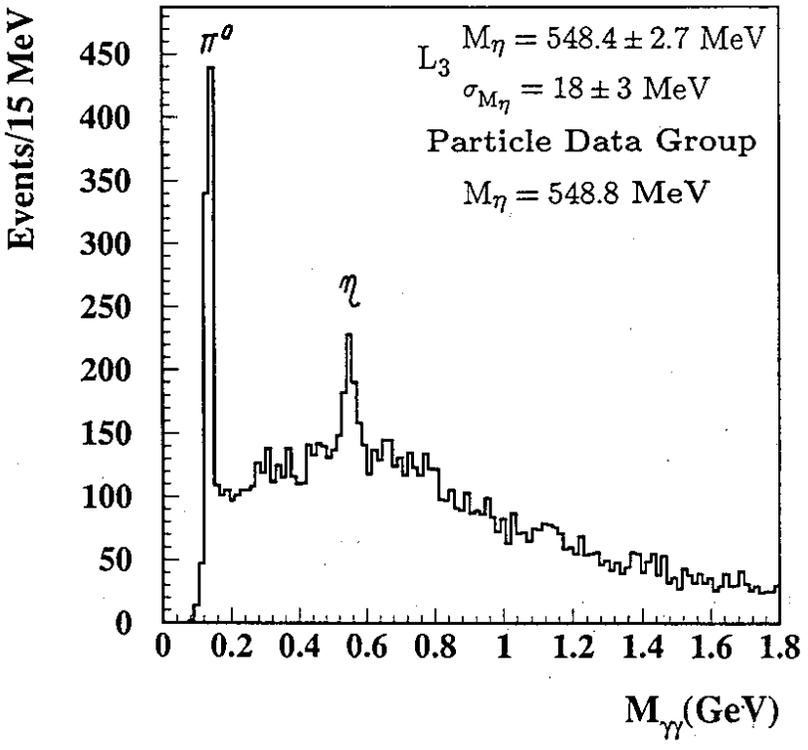

Figure 39: Invariant $\gamma\gamma$ mass spectrum, for isolated photons with $E_\gamma > 700$ MeV (L3)

4.17 Rare photonic Z decays

All four LEP Collaborations performed searches for rare photonic Z decays by looking for isolated photons. Naturally, L3 have an advantage there by virtue of the superb energy resolution of their BGO calorimeter. Figure 39 shows a promise of things to come in the future: their spectrum of invariant $\gamma\gamma$ masses, exhibiting prominent π^0 and η peaks. Table 18 summarizes the upper limits on rare photonic Z decays which have been achieved so far by the LEP Collaborations. The searches are limited by the integrated luminosity.

5 Summary

The amount of high-quality data, which has been accumulated in particular at LEP, in such a short time, is impressive. No less impressive is how well the Minimal Standard Model has been doing in defending itself.

The large amount of forthcoming data will significantly improve the level of precision of our knowledge of the electroweak and QCD sectors. Foreseeable limitations, from an insufficient un-

Table 18: Upper limits (95% CL) on the branching ratios of rare photonic Z decays (possible interference effects in the decay $Z \to \gamma^*\gamma$ have been ignored)

	Upper limits in units of 10^{-4}				
	$Z \to \pi^0\gamma$	$Z \to \eta\gamma$	$Z \to \eta'\gamma$	$Z \to \gamma^*\gamma$	$Z \to 3\gamma$
ALEPH [42]	4.9	4.6	2.2		0.45
DELPHI [64]	3.0	4.8			
L3 [44]	2.9	4.1		2.9	0.90
OPAL [46]	1.3	1.9		1.3	

derstanding of the Bhabha cross-section, and of higher-order QCD calculations, will hopefully be eliminated soon by further theoretical work.

The highlights of this first year of high-precision Z physics may be summarized as follows:

- $m_Z = 91.177 \pm 0.021$ GeV

  This measurement constitutes remarkable progress, and gives us, besides α and G_F, the third precisely measured cornerstone which is needed for precise theoretical predictions within the electroweak Standard Model.

- $N_\nu = 2.90 \pm 0.10$

- $\sin^2\bar{\theta}_w = 0.2301 \pm 0.0020$

  This determination from LEP data alone, is consistent with every other accepted measurement in the realm of electroweak physics. The value of $\sin^2\bar{\theta}_w$ is so precise that it is sensitive to $\mathcal{O}(\alpha)$ non-photonic radiative corrections, and helps significantly in constraining the t quark mass.

- $\alpha_s(m_Z^2) = 0.116 \pm 0.010$

  This determination of $\alpha_s(m_Z^2)$ from the jet multiplicity is consistent with the knowledge from other experiments but is plagued by large theoretical uncertainties.

- If the standard Higgs boson H^0 exists, the mass domain $0 \leq m_H \leq 44.0$ GeV is excluded at 95% CL.

- As for the discovery of new phenomena and/or new particles the reader may refer to Fig. 40, taken from a Singapore newspaper and slightly adapted.

Acknowledgement

I am greatly indebted to many colleagues who were extremely helpful in getting the material for this report together, and for a large number of enlightening discussions. Specific mention deserve the speakers of the LEP Collaborations: J.C. Brient, O. Callot, R. Geiges, J.R. Hansen, R. Johnson, T. Lohse, A. Roussarie, and K. Smith from ALEPH; W. Adam, U Amaldi, B. Koene, H. Müller, P. Renton, and R. Zitoun from DELPHI; J.G. Branson, M. Fukushima, T. Hebbeker, V. Innocente, P. McBride, H. Newman, and S.C.C. Ting for L3; A.H. Ball, A. Jawahery, R. Kowalewski, T. Mori,

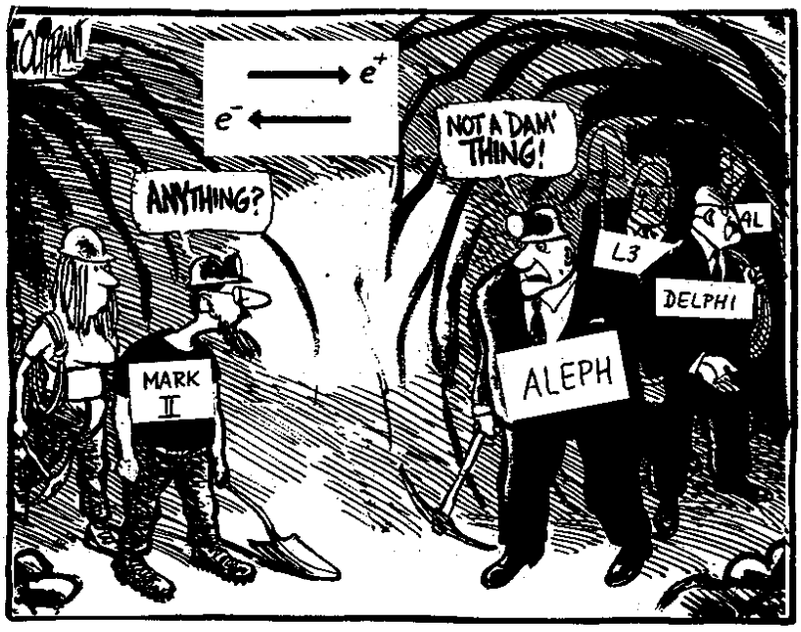

Figure 40: Ohne Worte

and K. Riles from OPAL. Particular thanks go to E. Fernandez, V. Innocente, C. Jarlskog, M. Martinez, S. Myers, L. Okun, L. Rolandi, V. Sharma, A. Wagner, and M. Winter. Thanks are due to J. Wotschack for his corrections of the manuscript, to my scientific secretary M. Thomson for his efficient and devoted assistance, to C. Rigoni for her skillful help with the drawings, and to J.M. Rabbinowitz and H. Mettler for their invaluable help with the editing.

References

[1] G.J. Feldman, Proc. Int. Symposium on Lepton and Photon Interactions at High Energies, Stanford, 1989, ed. M. Riordan (World Scientific, Singapore, 1990), p. 225.

[2] D.C. Kennedy and B.W. Lynn, Nucl.Phys. **B322** (1989) 1.

[3] G. Altarelli, Proc. Int. Symposium on Lepton and Photon Interactions at High Energies, Stanford, 1989, ed. M. Riordan (World Scientific, Singapore, 1990), p. 286.

[4] G. Burgers and W. Hollik, Program GAMMAZ.

[5] V. Hatton et al., LEP Absolute Energy in 1990, LEP Performance Note 12 (CERN, December 1990).

[6] M. Martinez et al., CERN preprint CERN-PPE/90-109 (1990).

[7] C. Jarlskog, talk presented at this conference; CERN preprint CERN-TH 5657/90 (1990).

[8] R. Johnson, talk presented at this conference.

[9] B. Adeva et al. (L3 Collaboration), L3 preprint No. 22 (1990).

[10] A. Jawahery, talk presented at this conference.

[11] J.R. Hansen, talk presented at this conference.

[12] J.C. Brient, talk presented at this conference.

[13] F. Dydak, Proc. of the Les Houches School, Session XLIV, 1985, eds. P. Ramond and R. Stora (Elsevier Science Publishers B.V., 1987), p. 127.

[14] P. Abreu et al. (DELPHI Collaboration), CERN preprint CERN-PPE/90-119 (1990).

[15] V. Innocente, private communication.

[16] T. Mori, talk presented at this conference.

[17] J. Alitti et al. (UA2 Collaboration), Phys. Lett. **B241** (1990) 150.

[18] F. Abe et al. (CDF Collaboration), Phys. Rev. Lett. **65** (1990) 2243.

[19] H. Abramowicz et al. (CDHS Collaboration), Phys. Rev. Lett. **57** (1986) 298; A. Blondel et al. (CDHS Collaboration), Z. Phys. **C45** (1990) 361.

[20] J.V. Allaby et al. (CHARM Collaboration), Phys. Lett. **B177** (1986) 446; Z. Phys. **C36** (1987) 611.

[21] M. Martinez, private communication.

[22] J. Ellis and G.L. Fogli, CERN preprint CERN-TH 5817/90 (1990).

[23] L. Pondrom, talk presented at this conference.

[24] P. Abreu et al. (DELPHI Collaboration), CERN preprint CERN-PPE/90-118 (1990).

[25] V. Innocente, talk presented at this conference.

[26] J.F. Kral et al. (MARK II Collaboration), Phys. Rev. Lett. **64** (1990) 1211.

[27] P. Abreu et al. (DELPHI Collaboration), CERN preprint CERN-PPE/90-123 (1990).

[28] R. Geiges, talk presented at this conference.

[29] B. Adeva et al. (L3 Collaboration), L3 preprint No. 20 (1990).

[30] C. Albajar et al. (UA1 Collaboration), Phys. Lett. **186B** (1987) 247; erratum ibid. **197B** (1987) 565.

[31] H. Albrecht et al. (ARGUS Collaboration), talk presented at this conference.

[32] M. Artuso et al. (CLEO Collaboration), Phys. Rev. Lett. **62** (1989) 2233.

[33] R.K. Ellis, D.A. Ross, and A.E. Terrano, Nucl. Phys. **178** (1981) 421.

[34] A. Bassetto, M. Ciafaloni and G. Marchesini, Phys. Rep. **100** (1983) 201.

[35] R.D. Field and P.P. Feynman, Nucl. Phys. **B136** (1978) 1.

[36] G. Ballocchi and R. Odorico, CERN preprint CERN-EP/89-162 (1989).

[37] B. Andersson et al., Phys. Rep. **97** (1983) 31.

[38] G. Marchesini and B.R. Webber, Nucl. Phys. **238** (1984) 1; **B238** (1984) 492.

[39] G. Gustafson and U. Petterson, Nucl. Phys. **B306** (1988) 746.

[40] T. Sjöstrand, Yellow Report CERN 89-08 (1990), Vol. 3, eds. G. Altarelli, R. Kleiss, and C. Verzegnassi.

[41] T. Hebbeker, talk presented at this conference.

[42] A. Roussarie, talk presented at this conference.

[43] B. Koene, talk presented at this conference.

[44] H. Newman, talk presented at this conference.

[45] G.S. Abrams et al. (MARK II Collaboration), Phys. Rev. Lett. **63** (1989) 2447.

[46] K. Riles, talk presented at this conference.

[47] K. Sliwa, talk presented at the XXVth Rencontre de Moriond on New Results in Hadronic Interactions, Les Arcs, France, March 1990.

[48] B. Adeva et al. (L3 Collaboration), L3 preprint No. 16 (1990)

[49] B. Adeva et al. (L3 Collaboration), Phys. Lett. **B247** (1990) 177; **B250** (1990) 205.

[50] D. Decamp et al. (ALEPH Collaboration), Phys. Lett. **B250** (1990) 172.

[51] B. Adeva et al. (L3 Collaboration), L3 preprint No. 21 (1990)

[52] D. Decamp et al. (ALEPH Collaboration), Phys. Lett. **B245** (1990) 289.

[53] P. Abreu et al. (DELPHI Collaboration), CERN preprint CERN-PPE/90-163 (1990).

[54] B. Adeva et al. (L3 Collaboration), L3 preprint No. 19 (1990).

[55] M.Z. Akrawy et al. (OPAL Collaboration), CERN preprint CERN-PPE/90-116 (1990).

[56] O. Callot, talk presented at this conference.

[57] M. Fukushima, talk presented at this conference.

[58] M.Z. Akrawy et al. (OPAL Collaboration), CERN preprint CERN-PPE/90-150 (1990).

[59] P. Fayet and S. Ferrara, Phys. Rep. **32** (1977) 249.

[60] B. Adeva et al. (L3 Collaboration), L3 preprint No. 15 (1990)

[61] B. Adeva et al. (L3 Collaboration), L3 preprint No. 18 (1990).

[62] A.H. Ball, talk presented at this conference.

[63] T. Barklow et al. (MARK II Collaboration), Phys. Rev. Lett. **64** (1990) 2984.

[64] P. Abreu et al. (DELPHI Collaboration), CERN preprint CERN-PPE/90-167 (1990).

[65] E. Soderstrom et al. (MARK II Collaboration), Phys. Rev. Lett. **64** (1990) 2980.

[66] M.Z. Akrawy et al. (OPAL Collaboration), CERN preprint CERN-PPE/90-132 (1990).

Imprimé au CERN. Prix : 1.30 Fr.